The Company of Biologists

RESEARCH ARTICLE

Pax9 is required for cardiovascular development and interacts with *Tbx1* in the pharyngeal endoderm to control 4th pharyngeal arch artery morphogenesis

Helen M. Phillips[1],[¶¶], Catherine A. Stothard[1],[¶¶], Wasay M. Shaikh Qureshi[1],[*], Anastasia I. Kousa[2], J. Alberto Briones-Leon[1], Ramada R. Khasawneh[1],[‡], Chloe O'Loughlin[1], Rachel Sanders[1],[§], Silvia Mazzotta[1],[¶], Rebecca Dodds[1], Kerstin Seidel[1],[**], Timothy Bates[3],[‡‡], Mitsushiro Nakatomi[1],[§§], Simon J. Cockell[4], Jürgen E. Schneider[5], Timothy J. Mohun[6], René Maehr[7], Ralf Kist[1],[3], Heiko Peters[1] and Simon D. Bamforth[1],[***]

ABSTRACT

Developmental defects affecting the heart and aortic arch arteries are a significant phenotype observed in individuals with 22q11 deletion syndrome and are caused by a microdeletion on chromosome 22q11. *TBX1*, one of the deleted genes, is expressed throughout the pharyngeal arches and is considered a key gene, when mutated, for the arch artery defects. *Pax9* is expressed in the pharyngeal endoderm and is downregulated in *Tbx1* mutant mice. We show here that *Pax9*-deficient mice are born with complex cardiovascular malformations that affect the outflow tract and aortic arch arteries with failure of the 3rd and 4th pharyngeal arch arteries to form correctly. Transcriptome analysis indicated that *Pax9* and *Tbx1* may function together, and mice double heterozygous for *Tbx1/Pax9* presented with a significantly increased incidence of interrupted aortic arch when compared with *Tbx1* heterozygous mice. Using a novel *Pax9Cre* allele, we demonstrated that the site of this *Tbx1-Pax9* genetic interaction is the pharyngeal endoderm, therefore revealing that a *Tbx1-Pax9*-controlled signalling mechanism emanating from the pharyngeal endoderm is required for crucial tissue interactions during normal morphogenesis of the pharyngeal arch artery system.

KEY WORDS: Pharyngeal endoderm, Arch artery development, *Tbx1*, *Pax9*, Neural crest, 22q11 deletion syndrome

[1]Institute of Genetic Medicine, Newcastle University, Newcastle-upon-Tyne NE1 3BZ, UK. [2]Memorial Sloan Kettering Cancer Center, New York, NY 10065, USA. [3]School of Dental Sciences, Newcastle University, Newcastle-upon-Tyne NE2 4BW, UK. [4]Bioinformatics Support Unit, Newcastle University, Newcastle-upon-Tyne NE2 4HH, UK. [5]Biomedical Imaging, University of Leeds, Leeds LS2 9JT, UK. [6]The Francis Crick Institute, London NW1 1AT, UK. [7]Diabetes Center of Excellence, University of Massachusetts Medical School, Worcester, MA 01605, USA.
*Present address: School of Biological Sciences, University of Manchester, Manchester M13 9PT, UK. ‡Present address: Yarmouk University, Irbid, Jordan. §Present address: The Queen's Medical Research Institute, University of Edinburgh, EH16 4TJ, UK. ¶Present address: TC BioPharm Limited, Motherwell ML1 4WR, UK. **Present address: Genentech, South San Francisco, CA 94080, USA. ‡‡Present address: Queen Elizabeth Hospital, Birmingham B15 2GW, UK. §§Present address: Kyushu Dental University, Kitakyushu 803-8580, Japan.

¶¶These authors contributed equally to this work

***Author for correspondence (simon.bamforth@newcastle.ac.uk)

H.M.P., 0000-0003-4513-9148; S.J.C., 0000-0002-6831-9806; J.E.S., 0000-0003-0999-5684; R.M., 0000-0002-9520-3382; R.K., 0000-0003-3729-5693; H.P., 0000-0002-9264-6532; S.D.B., 0000-0002-5666-4485

INTRODUCTION

Conotruncal heart malformations, which affect the outflow tract and aortic arch arteries, occur in 30% of all cases of congenital heart defects (Thom et al., 2006). Approximately 20% of foetuses identified with conotruncal defects by ultrasound are diagnosed with 22q11 deletion syndrome (22q11DS) (Boudjemline et al., 2001), the most common microdeletion syndrome with an incidence of 1:4000 live births (Scambler, 2000). Patients typically have a 3 Mb deletion on chromosome 22 that encompasses 45 protein-coding genes (Morrow et al., 2018) and ∼80% of patients present with some form of congenital cardiovascular defect (Momma, 2010), of which one of the most common observed is interruption of the aortic arch (IAA) (Unolt et al., 2018). Although clinically rare in the general population, ∼50% of all cases of IAA occur in 22q11DS patients (Boudjemline et al., 2001; Lewin et al., 1997; Van Mierop and Kutsche, 1986). IAA is a consequence of the left 4th pharyngeal arch artery (PAA) failing to form correctly during embryonic development. There are five pairs of PAAs that arise within a series of repeated protuberances on either side of the developing pharynx known as the pharyngeal arches. These arches consist of paraxial mesoderm- and neural crest cell (NCC)-derived mesenchyme, and are externally enclosed by ectoderm and internally lined by endoderm (Graham, 2003). The initially bilaterally symmetrical PAAs develop sequentially in a cranial to caudal sequence during embryogenesis but undergo a complex remodelling process, which is conserved in mammals, to form the asymmetrical mature aortic arch configuration (Bamforth et al., 2013; Hiruma et al., 2002). Of the genes deleted in 22q11DS, hemizygosity of *TBX1* is considered to be the cause of the cardiovascular defects, with point mutations in *TBX1* also identified in individuals with 22q11DS-like phenotypes (Yagi et al., 2003; Zweier et al., 2007). Tbx1 is expressed throughout the pharyngeal arches within the ectoderm, endoderm and mesoderm cells, and is crucial for pharyngeal arch and PAA development (Jerome and Papaioannou, 2001; Lindsay et al., 2001; Merscher et al., 2001). Complete loss of *Tbx1* from the mouse results in a failure of the pharyngeal arches to form correctly, resulting in hypoplasia of the second arch and aplasia of the remaining caudal arches, leading to an absent thymus and common arterial trunk (Jerome and Papaioannou, 2001; Merscher et al., 2001). In contrast, heterozygous deletion of *Tbx1* predominantly affects development of the 4th PAA resulting in IAA in a minority of mice with aberrant right-subclavian artery (A-RSA) observed more frequently (Lindsay et al., 2001). *Tbx1* heterozygotes may, however, also present with VSD, overriding aorta, double aortic arch and an abnormal thymus (Merscher et al., 2001; Zhang and Baldini, 2008). Although almost all 22q11DS patients are

1

hemizygous for the deletion, the phenotypic spectrum is highly variable (Unolt et al., 2018); thus, it has been proposed that genes outside of the deleted region may impact on the clinical phenotype (Guo et al., 2011b). Several genes have been identified as potential modifiers of 22q11DS, as determined by genetic interaction studies and transcriptome analyses in *Tbx1* mutant mice (Aggarwal and Morrow, 2008; Ivins et al., 2005; Liao et al., 2008; Papangeli and Scambler, 2013). One such candidate gene is *Pax9* the expression of which in the pharyngeal endoderm was found to be significantly reduced in *Tbx1*-deficient embryos (Ivins et al., 2005; Liao et al., 2008). *Pax9* belongs to a family of Pax genes encoding transcription factors involved in various cellular roles during embryonic development (Chi and Epstein, 2002; Mansouri et al., 1996) and is specifically expressed in the endoderm of all four pharyngeal pouches of the mouse by E9.5 (Neubüser et al., 1995). At later stages in mouse development, Pax9 is expressed in the oesophagus, somites and limbs, and within the neural crest contributing to craniofacial development (Peters et al., 1998). Embryos deficient for *Pax9* exhibit craniofacial defects, including a cleft secondary palate as well as absent teeth, skeletal defects and lack derivatives of the 3rd and 4th pharyngeal pouches, i.e. the thymus, parathyroids and ultimobranchial bodies (Peters et al., 1998), yet the role of Pax9 in cardiovascular development has not been determined.

In this study, we have investigated cardiovascular development in *Pax9*-deficient mice, and show that loss of *Pax9* leads to complex cardiovascular defects affecting the outflow tract and aortic arch arteries. We also uncover a strong genetic interaction between *Tbx1* and *Pax9* that leads to 4th PAA-derived defects in double heterozygous mice; this interaction is cell-autonomous within the pharyngeal endoderm.

RESULTS

Pax9-deficient embryos have cardiovascular defects

Mice lacking *Pax9* die perinatally and exhibit craniofacial, pharyngeal gland and skeletal defects (Peters et al., 1998). As the cause of death was unclear, we carefully re-analysed *Pax9*$^{-/-}$ neonates from a *Pax9*$^{+/-}$ intercross and found that all *Pax9*$^{-/-}$ neonates had a patterning defect of their aortic arch arteries that included an IAA with A-RSA (Fig. 1B; Table 1). To investigate these defects in more detail, we processed *Pax9*$^{-/-}$ embryos for histology and magnetic resonance imaging (MRI), and found that *Pax9*$^{-/-}$ embryos presented with a wide range of cardiovascular abnormalities (Fig. 1C-Q; Table 1). These defects included double outlet right ventricle with interventricular communication (Fig. 1F, J,K), IAA and A-RSA (Fig. 1G,K). The common carotid arteries were also frequently absent, resulting in unilateral or bilateral internal and external carotids arising directly from the dorsal aorta and the A-RSA (Fig. 1H,J-L). *Pax9*$^{-/-}$ embryos also had a hypoplastic aorta (Fig. 1N-O) and bicuspid aortic valves (Fig. 1Q).

Developmental defects of the arch arteries occur when the PAAs fail to form or remodel correctly. To investigate the morphogenesis of the PAAs, we performed high-resolution episcopic microscopy (HREM) on E10.5 and E11.5 *Pax9*$^{-/-}$ embryos and manually segmented the datasets to create 3D images of the PAA. Embryos were stage-matched by somite counting to exclude developmental delay as a cause of observed defects. Analysis of E10.5 coronal sections revealed that the 3rd and 4th pharyngeal arches of *Pax9*$^{-/-}$ embryos were smaller compared with *Pax9*$^{+/+}$ controls, as previously reported (Peters et al., 1998), but did show segmentation to individual arches (Fig. 2A-C). At E10.5, the developing PAAs are bilaterally symmetrical, having formed in a cranial to caudal sequence. The 1st and 2nd PAAs have normally

regressed by this stage, and the 3rd, 4th and 6th PAAs are present (Bamforth et al., 2013; Hiruma et al., 2002) (Fig. 2A). In *Pax9*$^{-/-}$ embryos, the 1st and 2nd PAAs were abnormally persistent, the 3rd PAAs were either absent, hypoplastic or interrupted, and the 4th PAAs were absent (Fig. 2B,C; Table 2). The aortic sac was also hypoplastic in *Pax9*$^{-/-}$ embryos compared with the controls (Fig. 2B,C). Intra-cardiac injection of India ink at E10.5-E11.0 showed that, in controls, the caudal PAAs were patent to ink and of equivalent size (Fig. 2D). In *Pax9*$^{-/-}$ embryos, however, persisting 1st and 2nd PAAs were patent to ink, and the 3rd PAAs were hypoplastic (Fig. 2J-L) or non-patent to ink, and therefore presumed absent. The majority of the 4th PAAs were bilaterally non-patent to ink (Fig. 2J-L; Table 2). Immunohistochemical staining for Pecam1 showed that the endothelium within the 3rd and 4th pharyngeal arches had formed lumenised PAAs at E10.5 in control embryos (Fig. 2G), but in *Pax9*$^{-/-}$ embryos the 3rd PAAs were visibly smaller in size and only isolated endothelial cells were seen within the 4th pharyngeal arch (Fig. 2H,I).

During E11.5 of mouse development, the PAA system begins to remodel and becomes asymmetric in appearance (Bamforth et al., 2013; Hiruma et al., 2002). In *Pax9* control embryos at this stage, the right 6th PAAs appeared thinner and the distal outflow tract was septated. The carotid duct, the region of the dorsal aorta between the 3rd and 4th PAAs, had begun to involute, but the 3rd, 4th and 6th PAAs remained connected to the dorsal aortae (Fig. 3A). In *Pax9*$^{-/-}$ embryos at E11.5, presumed persisting 1st or 2nd PAAs were observed extending anteriorly from the aortic sac, and the 3rd PAAs were also affected, either unilaterally or bilaterally, being either absent, hypoplastic or interrupted and not connected to the dorsal aortae (Fig. 3B-D). The carotid ducts were maintained, and this, coupled with the abnormal detachment of the 3rd PAAs from the dorsal aorta and the persistence of the 1st or 2nd PAAs, resulted in an absent common carotid artery and the internal and external carotid arteries arising directly from the aortic arch arteries, as observed at E15.5 (Fig. 1). Additionally, the distal outflow tract was unseptated and the 4th PAAs were bilaterally absent (Fig. 3B-D; Table 2).

Looping of the heart tube at E10.5 was not affected in *Pax9*$^{-/-}$ embryos (Fig. 3E,F).

In normal mouse development, the outflow tract cushions rotate through an anticlockwise direction (Bajolle et al., 2006), resulting in the major septal and parietal cushions being positioned side by side (Fig. 3G-I). In *Pax9*$^{-/-}$ embryos, however, by the end of the E11.5 stage these cushions were aberrantly positioned, with the parietal cushion more anterior to the septal cushion, indicating that a clockwise rotation of the outflow tract cushions had occurred (Fig. 3J-L).

Pharyngeal endoderm signalling influences neural crest cell differentiation

During normal embryogenesis, a subset of NCCs, the cardiac neural crest cells, migrate into the caudal pharyngeal arches to provide support to the developing PAAs and also contribute to outflow tract septation (Hutson and Kirby, 2003). *Pax9* is predominantly expressed in the pharyngeal endoderm (Fig. S1), but is also known to be expressed within the NCC and contributes to craniofacial development (Kist et al., 2007), although expression in cardiac NCC has not been described. We therefore looked to see whether a cell-autonomous loss of *Pax9* from NCC resulted in cardiovascular defects. Conditional deletion of *Pax9* using *Wnt1Cre* transgenic mice (Danielian et al., 1998), and the *Pax9*^{flox} allele (Kist et al., 2007), however, did not result in cardiovascular abnormalities,
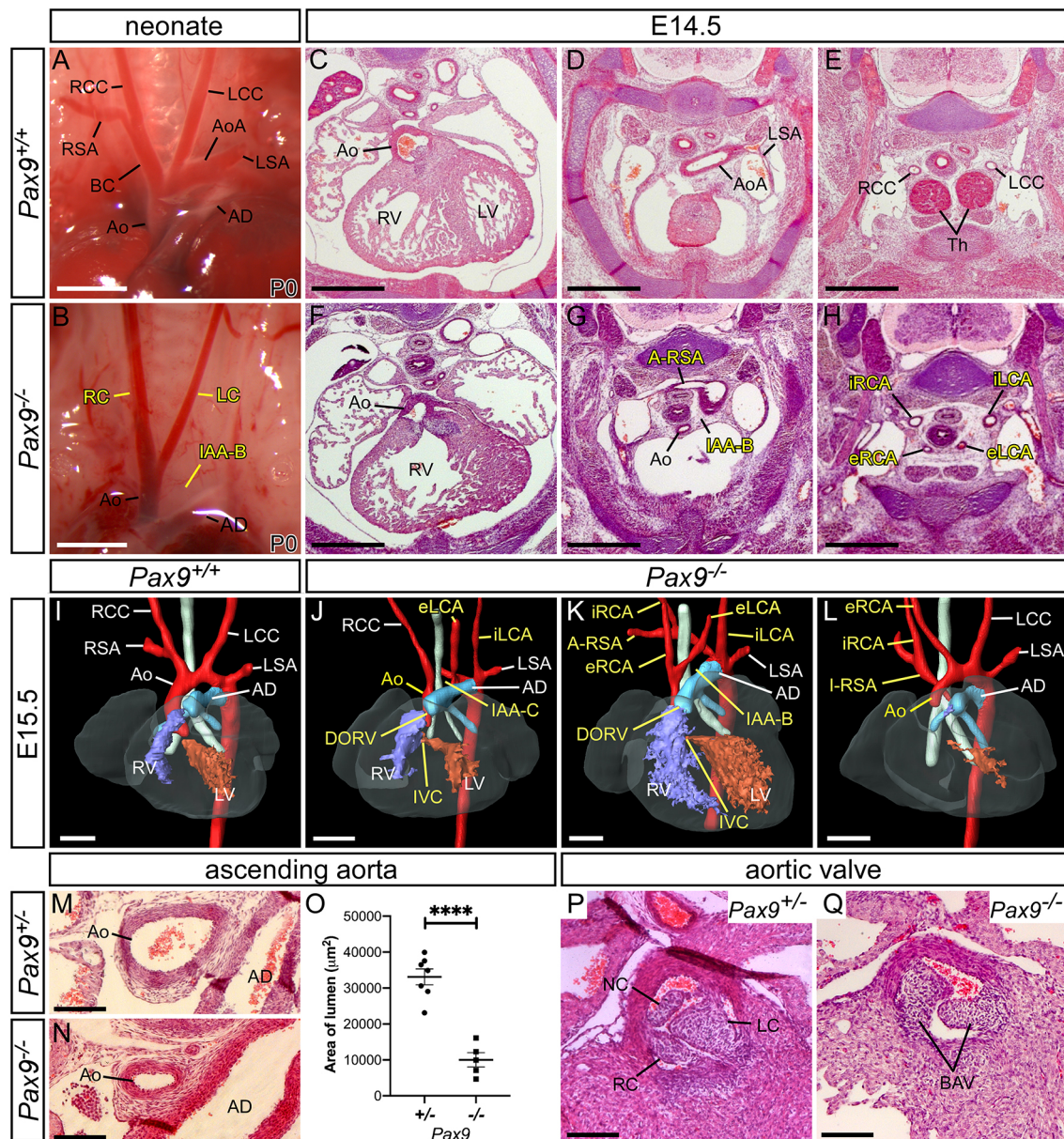
Fig. 1. Loss of Pax9 results in cardiovascular developmental defects. (A) Arch arteries of control neonates were normal (*n*=8). (B) *Pax9*−/− neonates (*n*=5) displayed IAA-B, absent right subclavian artery (presumed retro-oesophageal), and atypical right and left carotid arteries (LC and RC). Scale bars: 1 mm. (C-E) *Pax9*+/+ embryos at E14.5 show normal outflow tract, arch arteries and thymus. (F-H) In *Pax9*−/−embryos (*n*=4), the aorta (Ao) arises aberrantly from the right ventricle producing a double outlet right ventricle (DORV; F). Hypoplastic aorta, IAA-B and an A-RSA are present (G). More cranially, the thymus is absent and aberrant internal and external carotid arteries (iRCA, eRCA, iLCA, eLCA) are seen (H). (I-L) 3D reconstructions of E15.5 hearts from MRI datasets. (I) *Pax9*+/+ embryo with normal aortic arch arteries. (J-L) In *Pax9*−/−embryos (*n*=15), defects seen are DORV with interventricular communication (IVC), IAA (type B or C), A-RSA (retro-esophageal in J,K and isolated in L) and aberrant carotid arteries. Scale bars: 500 μm. (M-O) The ascending aorta is significantly smaller in *Pax9*−/− embryos (*n*=5) compared with *Pax9*+/− control embryos (*n*=7). Data are mean±s.e.m. ****P<0.0001 (two-tailed unpaired *t*-test). (P) *Pax9*+/− control embryos have three normal aortic valve leaflets (*n*=6): the right (RC), left (LC) and non-coronary (NC). (Q) *Pax9*−/− embryos (*n*=5) have bicuspid aortic valve (BAV). Scale bar: 100 μm. AoA, aortic arch; AD, arterial duct; BC, brachiocephalic; dAo, dorsal aorta; LCC, left common carotid artery; LSA, left subclavian artery; LV, left ventricle; RCC, right common carotid artery; RSA, right subclavian artery; RV, right ventricle.

although cleft palate was observed as expected (Fig. 4A-D). We next looked to see whether the migration of NCCs was affected in global *Pax9*−/− embryos using *Wnt1Cre* and *eYFP* (Srinivas et al., 2001) reporter mice to create embryos where the NCC could be lineage traced. Live fluorescence imaging of *Pax9*+/+;*Wnt1Cre;eYFP* embryos at E9.5 and E10.5 revealed NCCs present in the head and dorsal root ganglia, as well as migrating towards and filling the pharyngeal arches (Fig. 4E,G). A similar pattern was observed in *Pax9*−/−;*Wnt1Cre;eYFP* embryos (Fig. 4F,H). Counting of NCCs revealed no significant change in their number in the 3rd pharyngeal arch at E9.5, but a significant reduction was found in the 3rd and 4th arches at E10.5 (Fig. 4K). Immunostaining for BrdU incorporation specifically in NCCs showed no significant difference in NCC proliferation in the caudal pharyngeal arches (Fig. 4L-N), and very little apoptosis was seen in both control and *Pax9*−/− embryos (Fig. 4O-Q). These observations indicated that the migration of NCCs per se to the pharyngeal arches was not affected in *Pax9*−/− embryos. Given that NCCs differentiate into the smooth muscle

Table 1. Number of cardiovascular defects observed in mutant embryos (>E13.5) and neonates

Genotype	Stage	n	VSD	DORV+IVC	IAA[‡]	IAA+A-RSA[§]	A-RSA[§]	Vascular ring[¶]	Cervical AoA+A-RSA	Absent CC[‡‡]
Pax9−/−	Neonatal	5	NA	NA	0	5 (100%)	0	0	0	2 (40%)
	E14.5-E15.5	19	3 (16%)	15 (79%)	3 (16%)	14 (74%)	2 (11%)	0	0	15 (79%)
Tbx1+/−	Neonatal	6	NA	NA	0	1 (17%)	3 (50%)	0	0	0
Tbx1+/−; Pax9+/−		9			1 (11%)	5 (55%)	2 (22%)	0	1 (11%)	0
Tbx1+/−	E15.5	19	0	0	0	1 (5%)	9 (47%)	0	2 (11%)	0
Tbx1+/−; Pax9+/−		20	6* (30%)	0	0	14** (70%)	3 (15%)	0	3 (15%)	0
Tbx1+/flox; Pax9Cre	Neonatal	8	0	0	0	0	4 (50%)	1 (12.5%)	0	0
	E13.5-E15.5	26	0	0	0	1 (4%)	6 (23%)	3 (11.5%)	0	0

*Pax9−/− neonates (n=5) were analysed by dissection, embryos at E14.5 by histology (n=4) and at E15.5 by MRI (n=15). Tbx1+/− (n=19) and Tbx1+/−;Pax9+/− (n=20) embryos were analysed by MRI. Tbx1+/flox;Pax9Cre embryos were analysed by MRI (n=17) and µCT (n=9). All wild-type (n=16), Pax9+/− (n=15) and Tbx1+/flox (n=5) control embryos assessed were normal. There was a statistically significant increase in the incidence of VSD and IAA in the Tbx1+/−;Pax9+/− embryos compared with the Tbx1+/− embryos. *P<0.05, **P<0.0001 (Pearson's chi-squared test for associations).*
[‡]Combined incidence of IAA, irrespective of co-occurrence with A-RSA, in Pax9−/− neonates and embryos (n=24) was 92% (n=19 type-B and n=3 type-C). In Tbx1 mutants, IAA was always type B.
[§]A-RSA refers to a retro-oesophageal, cervical origin or isolated right subclavian artery. Two Pax9−/− embryos had isolated RSA.
[¶]Vascular ring is used to describe a right-sided aorta with A-RSA.
[‡‡]Absent common carotid artery (CC), resulting in the internal and external carotid arteries arising directly from the main aortic vessels, unilaterally (n=4) or bilaterally (n=11) in Pax9−/− embryos.
AoA, aortic arch; DORV+IVC, double outlet right ventricle with interventricular communication; VSD, perimembranous ventricular septal defect; NA, not assessed.

cells (SMCs) that support the remodelling PAAs (Waldo et al., 1996), we looked to see whether SMC recruitment to the 3rd PAAs was affected in *Pax9−/−* embryos. Sections from E10.5 and E11.5 embryos were immunostained using an anti-alpha smooth muscle actin antibody to visualise SMCs around the PAAs. Evidence of SMC recruitment to the 3rd PAAs was seen in each control embryo examined (Fig. 4R-U); however, very little SMC recruitment to the 3rd PAAs in *Pax9−/−* embryo sections was observed (Fig. 4V-Y).

These results indicate that the 3rd PAAs in *Pax9−/−* embryos form but collapse from a failure of SMC recruitment.

Tbx1 and *Pax9* interact in 4th PAA formation
To further investigate the role of *Pax9* in cardiovascular development, we looked at the effect of *Pax9* loss on the pharyngeal arch transcriptome at E9.5 (Fig. 5A-C). Analysis of the RNA-seq data identified 3863 significant differentially expressed genes (Table S1).
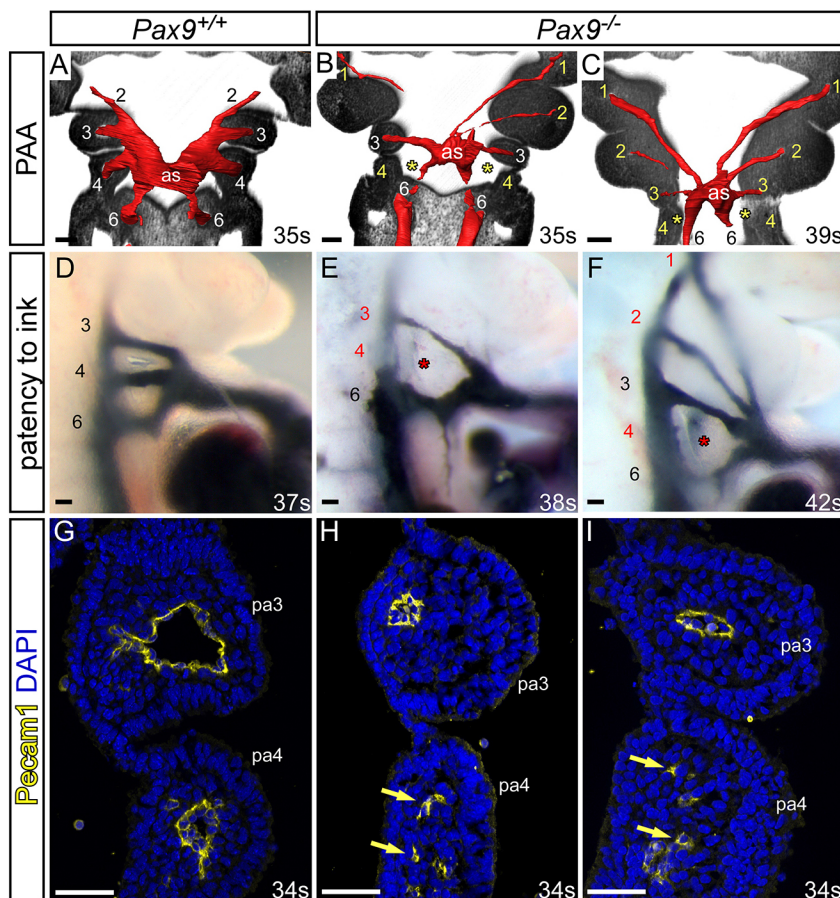
Fig. 2. Pax9 loss causes aberrations in pharyngeal arch artery formation. (A-C) Coronal views of control (*Pax9+/+*) and mutant (*Pax9−/−*) embryos at E10.5 (30-40 s), examined by high-resolution episcopic microscopy. (A) In *Pax9+/+* control embryos (n=5), the 3rd, 4th and 6th PAAs are of equal size and bilaterally symmetrical. (B,C) In *Pax9−/−* embryos (n=4), the 4th PAAs were bilaterally absent (asterisk), the 3rd PAAs and aortic sac (as) were hypoplastic, and the 1st and/or 2nd PAAs abnormally persisted. (D-F) Intracardiac ink injection into E10.5-E11.0 (31-42 s) embryos. (D) In control embryos (n=12), PAAs 3-6 are patent to ink, are of equivalent diameter and are bilaterally symmetrical. (E,F) In *Pax9−/−* embryos (n=12), the 3rd PAAs are hypoplastic and the 4th PAAs are non-patent to ink (asterisk). (F) The 1st and 2nd PAAs are persisting anomalously. (G-I) Immunostaining using anti-Pecam1 antibody at E10.5 (31-36 s). (G) Control embryos (n=3) have a ring of Pecam1-positive endothelium lining the 3rd and 4th PAAs. (H,I) In *Pax9−/−* embryos (n=5), the 3rd PAAs are visibly smaller and disorganized endothelial cells are within the 4th pharyngeal arch (pa; arrows). Somite counts (s) are indicated. Scale bars: 100 µm. The somite numbers given in the legend reflect the range analysed for the whole study. The figure contains representative images only.

Table 2. Number of pharyngeal arch artery defects

| Genotype	n	PAA	Abnormal (%)	Unilateral defect	Bilateral defect	Bilateral defects Present	Hypo/Int/Abs	Absent
$Pax9^{-/-}$	20	1	11 (55%)	1	10	9	1	0
		2	8 (40%)	3	5	4	1	0
		3	15 (75%)	3	12	-	8	4
		4	20 (100%)	1	19	-	3	16
$Tbx1^{+/-}$	8	4	8 (100%)	4	4	-	4	0
$Tbx1^{+/-}; Pax9^{+/-}$	9	4	9 (100%)	1	8	-	1	7*
$Tbx1^{+/flox}$	15	4	0	0	0	-	0	0
$Tbx1^{+/flox}; Pax9Cre$	17	4	16 (92%)	3	13	-	7	6

Embryos were collected and assessed for PAA defects. $Pax9^{-/-}$ embryos were either injected intracardially with ink (E10.5; n=12) or imaged using HREM (E10.5-E11.5; n=8) to visualise the PAA. Data are combined. For $Pax9^{-/-}$ embryos, each left and right PAA 1-4 was scored as having a unilateral or bilateral defect, and the bilateral defects categorised as either present, a combination of hypoplastic, interrupted and/or absent (Hypo/Int/Abs), and bilaterally absent. For $Tbx1;Pax9$ genotypes, ink injection was performed at E10.5 and only the 4th PAA was scored. The increase in bilaterally absent 4th PAA in $Tbx1^{+/-};Pax9^{+/-}$ embryos is significant compared with $Tbx1^{+/-}$ embryos. *P=0.004 (Pearson's chi-squared test for associations). All control $Pax9^{+/+}$ (n=18) and $Pax9^{+/-}$ (n=25) embryos were normal.

Gene set enrichment analysis revealed several significantly downregulated pathways, including 'extracellular matrix organisation' and 'axon guidance' (Fig. 5D). Interestingly, $Tbx1$ was significantly reduced in $Pax9^{-/-}$ embryos at E9.5, and this was confirmed by qPCR (Fig. 5I). We also confirmed that $Pax9$ expression was reduced in $Tbx1$-null embryos (Fig. S2). As $Tbx1$ expression is crucial for 4th PAA morphogenesis (Lindsay et al., 2001; Zhang et al., 2005), these data suggested that $Pax9$ may function together with $Tbx1$ rather than being downstream of it. We therefore compiled a list of all the genes reported to be significantly
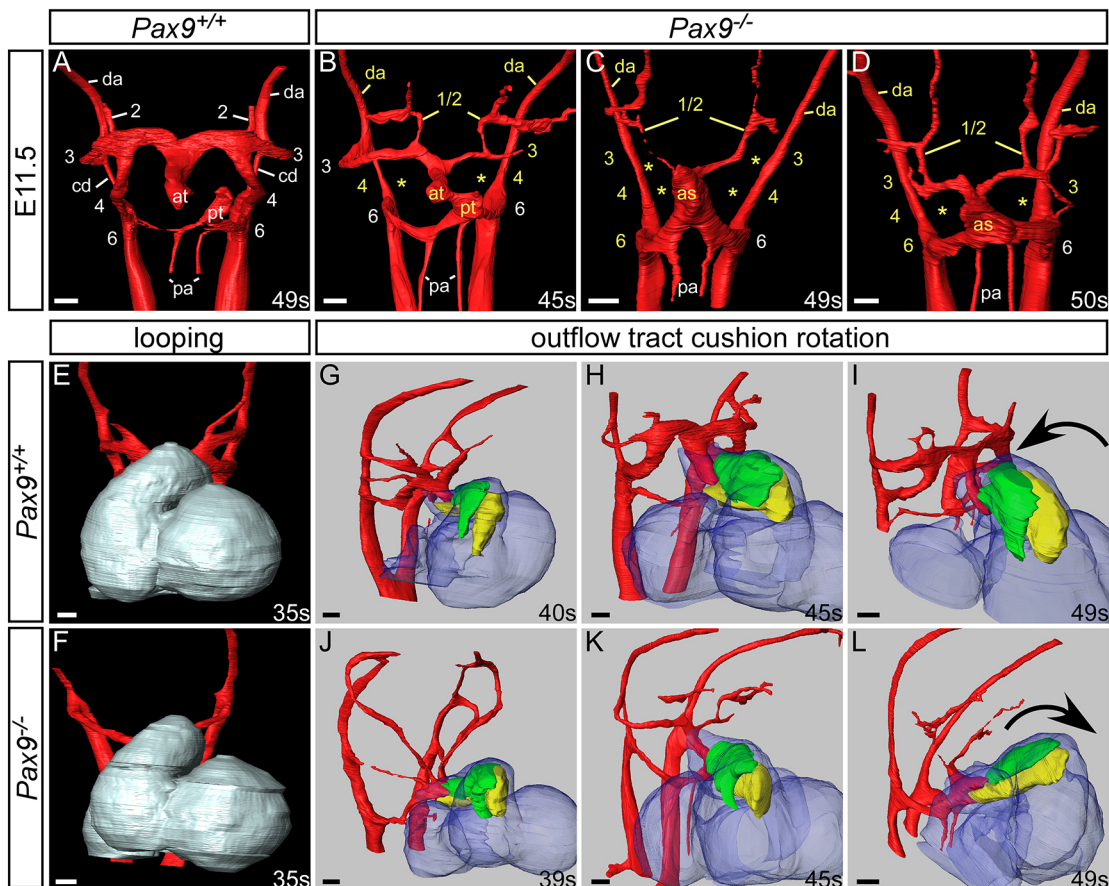

Fig. 3. $Pax9^{-/-}$ embryos display aberrant rotation of the outflow tract and abnormal PAA remodelling. Image datasets were acquired by high-resolution episcopic microscopy. (A-D) 3D reconstructions of the PAAs at E11.5 (45-50 s). (A) In $Pax9^{+/+}$ control embryos (n=5), the outflow tract is septated, the right 6th PAA has thinned and the carotid duct (cd) has begun to involute. (B-D) In $Pax9^{-/-}$ embryos (n=4), the 4th PAAs are absent and the 3rd PAAs are aberrantly connected or detached from the dorsal aorta (da; asterisks). The carotid duct has failed to involute and septation of the outflow tract is delayed. Persisting 1st or 2nd PAAs are observed coursing anteriorly from the abnormal 3rd PAAs (B,D) or from the aortic sac (as; C). (E,F) Looping of the heart tube at E10.5 was not affected in $Pax9^{-/-}$ embryos (n=4). (G-L) Outflow tract rotation from E10.5 to E11.5 (39-49 s). (G-I) In control embryos, the major outflow tract cushions (parietal in green; septal in yellow) rotated in an anti-clockwise direction, resulting in the cushions being aligned side by side. (J-L) In $Pax9^{-/-}$ embryos, the cushions rotated in a clockwise direction, resulting in the parietal cushion being anterior to the septal cushion. at, aortic trunk; pa, pulmonary arteries; pt, pulmonary trunk. Somite (s) counts indicated. Scale bars: 100 μm.

5
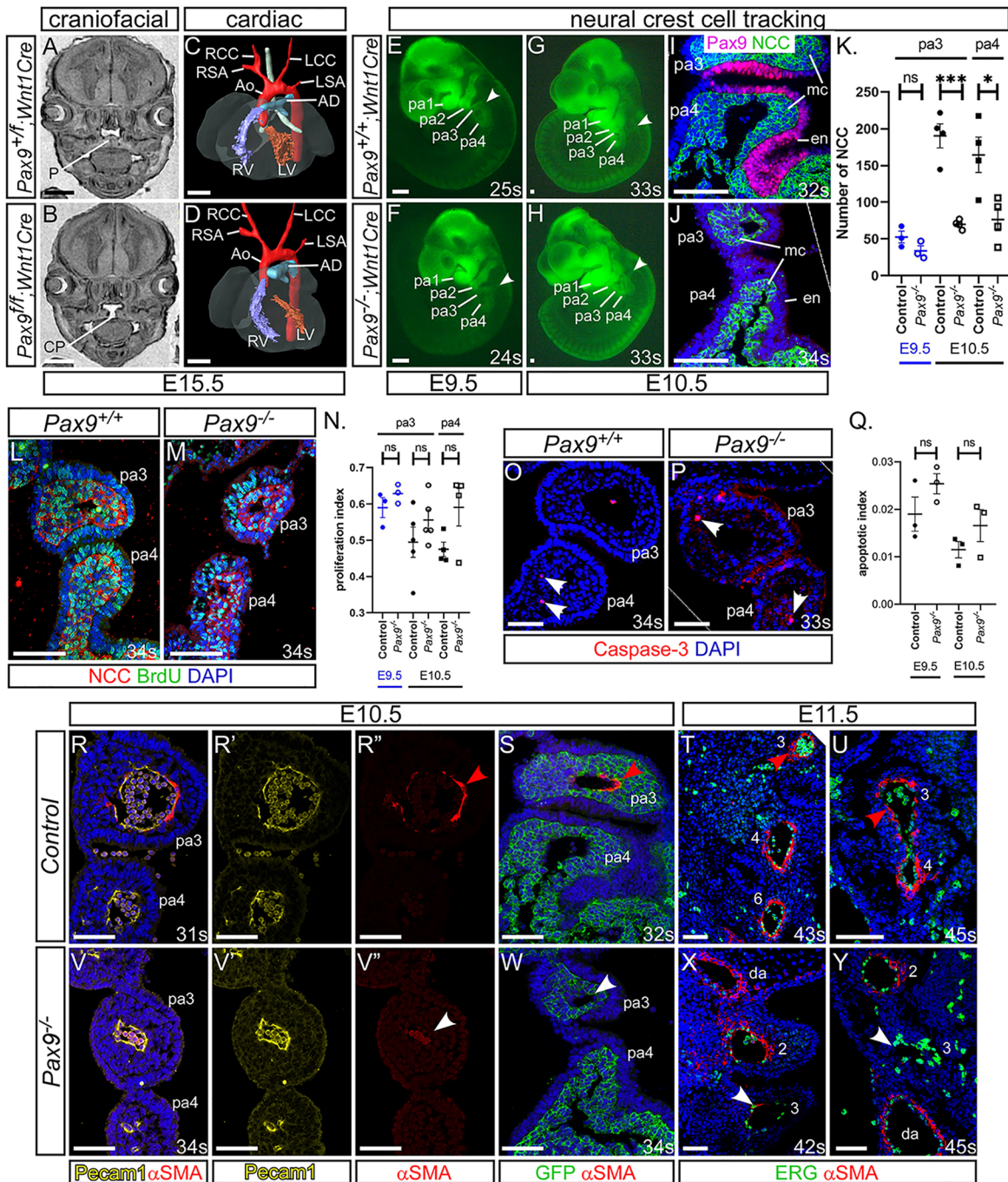
Fig. 4. Failure in smooth muscle cell recruitment causes the 3rd PAAs to collapse. (A-D) E15.5 embryos with a *Pax9* conditional deletion in neural crest cells (NCCs) were examined by MRI. (A) Control embryos had a normal palate (P). (B) *Pax9^f/f^;Wnt1Cre* mutant embryos (*n*=6) had cleft palate (CP). (C,D) No cardiovascular defects were observed in control or mutant embryos. Ao, aorta; AD, arterial duct; LCC, left common carotid artery; LSA, left subclavian artery; LV, left ventricle; RCC, right common carotid artery; RSA, right subclavian artery; RV, right ventricle. (E-J) NCCs in *Pax9^+/+^* (E,G,I) or *Pax9^−/−^* (F,H,J) embryos were labelled using *Wnt1Cre* and *eYFP* alleles. (E-H) Fluorescence imaging showed no difference in NCC migration into the pharyngeal arches (arrowheads) at E9.5 (*n*≥3, 23-25 s) and E10.5 (*n*≥5, 32-36 s). (I,J) Fluorescent embryos were sectioned coronally and immunostained using anti-GFP and anti-Pax9 antibodies. (K) NCCs were counted from immunostained sections. *P<0.05, ***P<0.001 (two-tailed unpaired *t*-test). (L,M) Embryo sections were immunostained with anti-BrdU and anti-GFP antibodies to detect proliferation in NCCs in *Pax9^+/+^* (L) and *Pax9^−/−^* (M) embryos. (N) No significant difference in the rate of proliferation was found between control and *Pax9^−/−^* NCCs in the caudal arches at E9.5 (*n*=3, 23-28 s) or E10.5 (*n*≥4, 31-39 s). (O,P) Embryo sections immunostained using an anti-caspase 3 antibody to detect apoptosis in the caudal pharyngeal arches of *Pax9^+/+^* (N,O) and *Pax9^−/−^* (P) embryos. (Q) No significant difference in the rate of apoptosis was found between control and *Pax9^−/−^* embryos at E9.5 (*n*=3, 24-28 s) or E10.5 (*n*=3, 30-35 s). Two-tailed unpaired *t*-test. (R-Y) Embryo sections were immunostained using anti-αSMA antibody for smooth muscle (R,R″-U,V,V″-Y,S,W), anti-Pecam1 (R,R′,V,V′) or -ERG (T,U,X,Y) antibodies for endothelium, or anti-GFP to label NCCs in *Wnt1Cre;eYFP* embryos (S,W). In all control embryos, SMC surrounded the 3rd PAAs [E10.5, *n*=7, 31-36 s (R,S); and E11.5, *n*=3, 43-45 s (T,U); red arrowhead]. In *Pax9^−/−^* embryos, the 3rd PAAs had limited recruitment of SMCs [E10.5, *n*=6; 32-35 s (V,W); and E11.5, *n*=3, 42-45 s (X,Y); white arrowheads]. da, dorsal aorta; en, endoderm; mc, mesenchyme; ns, not significant; pa, pharyngeal arch. Somite counts (s) are indicated. Scale bars: 500 μm in A-D; 100 μm in E-J,L,M,O,P; 50 μm in R-Y. The somite numbers given in the legend reflect the range analysed for the whole study. The figure contains representative images only.
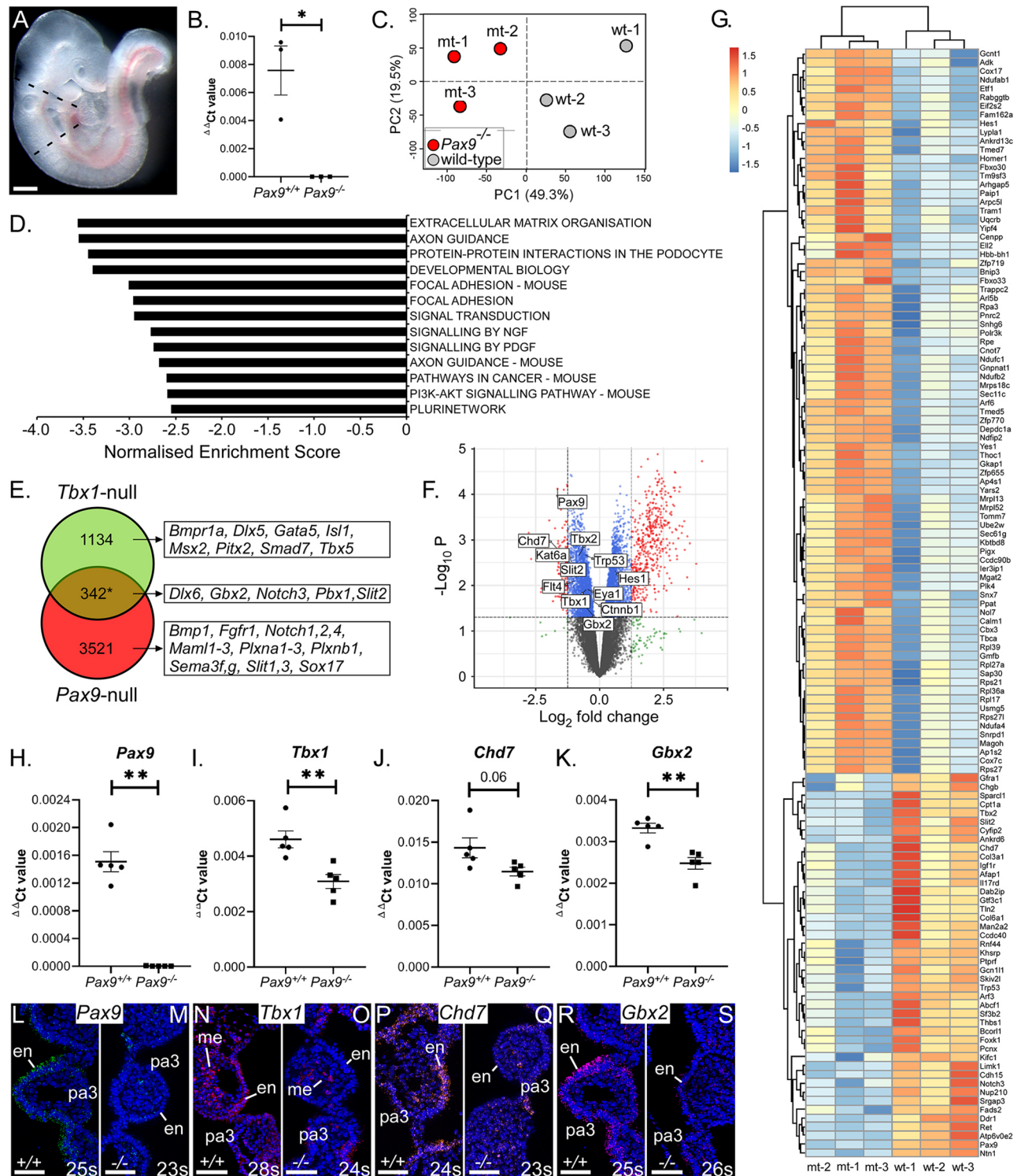
Fig. 5. *Pax9* shares a genetic network with *Tbx1*. (A) The pharyngeal arch region of control and *Pax9*$^{-/-}$ embryos at E9.5 (*n*=3 per genotype; 26-27 s) was dissected (indicated by dashed lines). Scale bar: 500 μm. (B) Total RNA was extracted, converted to cDNA and checked by qPCR. (C) Principle component analysis of RNA-seq data showed a clear separation between control and mutant samples (shown on PC2) and only slight biological variation across replicates (shown on PC1). (D) Gene set enrichment analysis identified signalling pathways predicted to be significantly downregulated in *Pax9*$^{-/-}$ embryos. All pathways shown have a familywise-error rate of *P*<0.001. (E) *Tbx1*-related genes (*n*=1476) were compared with those genes significantly differentially expressed (DE) in *Pax9*$^{-/-}$ embryo tissue (*n*=3863, adjusted *P*≤0.1) giving 342 genes common to both datasets (**P*=0.0029, as assessed by a hypergeometric distribution test). Examples of genes in each cohort are shown. (F) Volcano plot highlighting *Tbx1*-interacting genes significantly DE in *Pax9*$^{-/-}$ embryos (based on adjusted *P*≤0.1). (G) Heat map showing colour-coded (red, up; blue, down) expression levels of DE genes between *Pax9*$^{+/+}$ (wt) and *Pax9*$^{-/-}$ (mt) embryos that are common to *Tbx1* DE genes (adjusted *P*≤0.05 are shown). (H-K) qPCR analysis confirmed that *Pax9* (H), *Tbx1* (I), *Chd7* (J) and *Gbx2* (K) were significantly reduced in *Pax9*$^{-/-}$ pharyngeal tissue at E9.5 (*n*=5 embryos per genotype). **P*<0.01; two-tailed unpaired *t*-test (*Tbx1* and *Chd7*) and two-tailed Mann–Whitney (*Pax9* and *Gbx2*). (L-S) RNAscope *in situ* hybridisation showed a reduced expression of *Pax9* (M), *Tbx1* (O), *Chd7* (Q) and *Gbx2* (S) in the pharyngeal endoderm in *Pax9*$^{-/-}$ embryos at E9.5 (*n*=3 per genotype, 23-28 s). en, endoderm; me, mesoderm; pa, pharyngeal arch. Somite counts (s) are indicated. Scale bars: 50 μm.

differentially expressed in *Tbx1*-null embryos from published microarray (Ivins et al., 2005; Liao et al., 2008; van Bueren et al., 2010) and mouse genetic interaction studies, giving 1476 unique *Tbx1*-related genes. These were then compared with all genes significantly changed in *Pax9*−/− embryo pharyngeal arch tissue, giving 342 genes that were common to both datasets (Fig. 5E-G; Fig. S3; Table S1) and suggesting that *Tbx1* and *Pax9* may share a genetic network. Among these common genes were *Chd7* and *Gbx2*, which have been shown to interact with *Tbx1* in mice (Calmont et al., 2009; Randall et al., 2009), and were also reduced in *Pax9*-null tissue by qPCR and *in situ* hybridisation (Fig. 5H-S).

To investigate a potential genetic interaction *in vivo* between *Tbx1* and *Pax9*, we confirmed that both genes were co-expressed in

the pharyngeal endoderm (Fig. 6A-G). We then crossed *Tbx1*+/− mice (Jerome and Papaioannou, 2001) with *Pax9*+/− mice to create *Tbx1*+/−;*Pax9*+/− double heterozygotes. Genotype analysis of 168 pups at weaning revealed that only two *Tbx1*+/−;*Pax9*+/− mice were alive, a highly significant deviation from the 42 expected of each genotype from this cross ($P=1.4\times10^{-12}$; Table S2). To identify the timing of lethality, neonates were observed from the day of birth with all *Tbx1*+/−;*Pax9*+/− mutants dying during the first 24 h. Examination of neonatal aortic arch arteries revealed that all controls were normal (Fig. 6H), while *Tbx1*+/− neonates frequently presented with A-RSA (Fig. 6I; Table 1). All dead *Tbx1*+/−;*Pax9*+/− neonates had 4th PAA-derived defects, including IAA (Fig. 6J,K; Table 1).
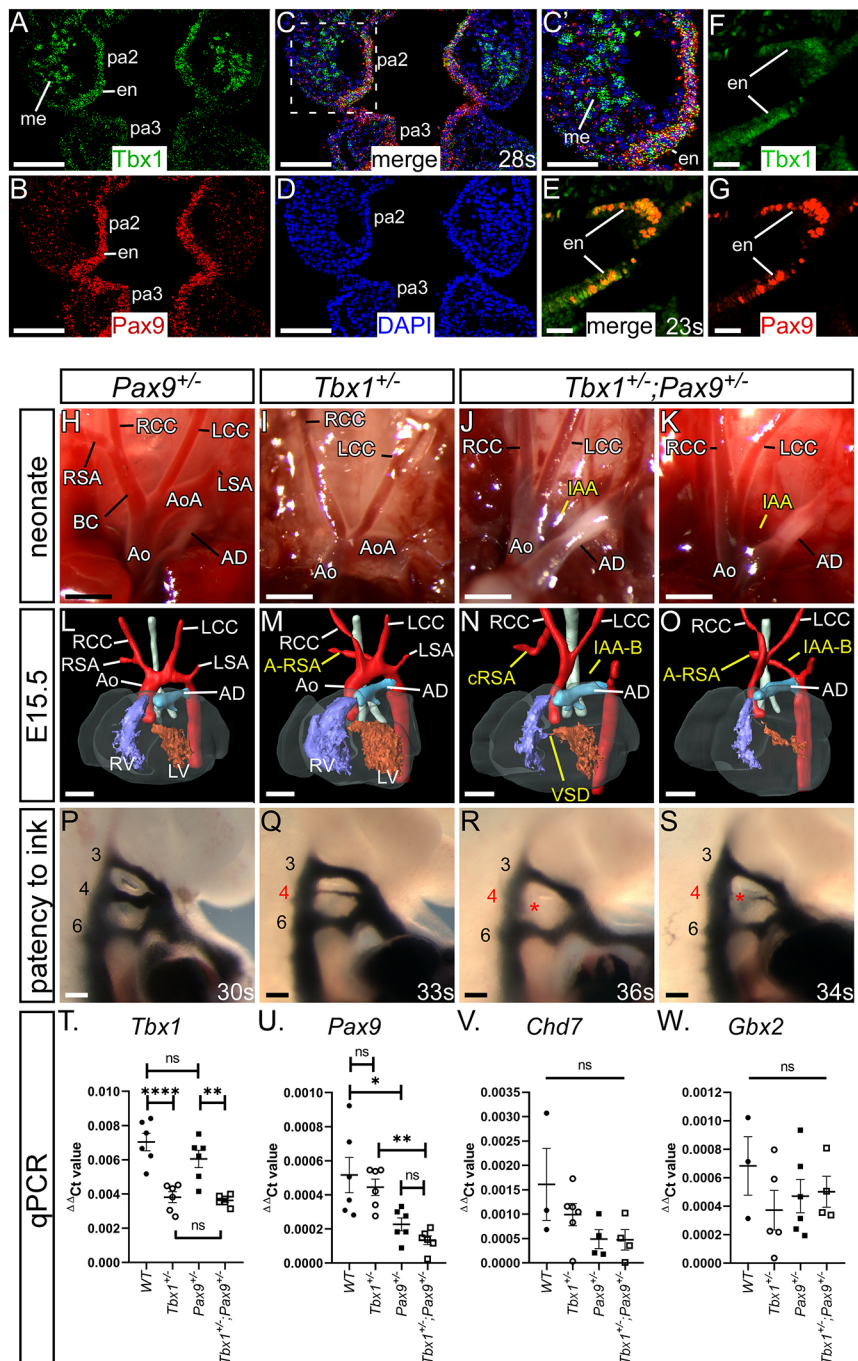
Fig. 6. *Tbx1;Pax9* double heterozygous embryos have 4th PAA defects. *Tbx1* and *Pax9* expression in the pharyngeal arches was examined at E9.5. (A-D) RNAScope *in situ* hybridisation expression of *Tbx1* in the 2nd and 3rd pharyngeal arch (pa), endoderm (en) and mesoderm (me; A), and *Pax9* expression in the endoderm only (B). The signals overlap in the endoderm (C, and higher power in C′). (D) DAPI staining. (E-G) Immunostaining for Tbx1 and Pax9 (E) demonstrates protein colocalisation within cells of the pharyngeal endoderm. Single staining for Tbx1 (F) and Pax9 (G) is shown. (H-K) Neonates from a *Tbx1*+/− and *Pax9*+/− intercross were recovered and the aortic arches examined. (H) Arch arteries were normal in all *Pax9*+/− neonates (n=10). (I) *Tbx1*+/− neonates (n=6) often presented with A-RSA, inferred by the absence of the brachiocephalic and right subclavian arteries. (J,K) All *Tbx1*+/−; *Pax9*+/− neonates (n=9) died within 24 h of birth with IAA and/or A-RSA. (L-O) 3D reconstructions of E15.5 embryo hearts from MRI datasets. (L) *Pax9*+/− hearts were normal (n=15). (M) *Tbx1*+/− hearts (n=19) frequently displayed 4th PAA defects such as A-RSA. (N,O) All *Tbx1*+/−; *Pax9*+/− embryos (n=20) presented with a 4th PAA-derived defect such as IAA-B, A-RSA and/or cervical right subclavian artery (cRSA). (P-S) Intracardiac ink injections into E10.5 embryos (27-38 s). (P) PAAs in control embryos were normal (n=10). (Q) In *Tbx1*+/− embryos (n=8) the 4th PAAs were often hypoplastic. (R,S) In *Tbx1*+/−;*Pax9*+/− embryos (n=9), the 4th PAAs were frequently bilaterally absent. Ao, aorta; AoA, aortic arch; AD, arterial duct; BC, brachiocephalic; LCC, left common carotid artery; LSA, left subclavian artery; LV, left ventricle; RCC, right common carotid artery; RSA, right subclavian artery; RV, right ventricle. Somite counts (s) are indicated. Scale bars: 2 mm in H-K; 500 μm in L-O; 100 μm in A-D,P-S; 50 μm in E-G. (T-W) qPCR analysis in wild-type, *Tbx1*+/−, *Pax9*+/− and *Tbx1*+/−;*Pax9*+/− embryos (n≥3 per genotype, somite range 23-27). (T) *Tbx1* levels were significantly reduced in *Tbx1*+/− and *Tbx1*+/−;*Pax9*+/− embryos. (U) *Pax9* levels were significantly reduced in *Pax9*+/− and *Tbx1*+/−; *Pax9*+/− embryos. There was no significant difference in *Tbx1* (T), *Pax9* (U), *Chd7* (V) or *Gbx2* (W) levels between single heterozygotes and *Tbx1*+/−;*Pax9*+/− embryos. One-way ANOVA with Tukey's multiple comparison test. ns, not significant. *P<0.05, **P<0.01, ****P<0.0001.

DEVELOPMENT

Having established postnatal cardiovascular defects, we next analysed E15.5 *Tbx1*$^{+/-}$;*Pax9*$^{+/-}$ embryos by MRI (Fig. 6L-O). All wild-type and *Pax9*$^{+/-}$ embryos were normal. Of the *Tbx1*$^{+/-}$ embryos examined, a high proportion had some form of 4th PAA-derived defect, including IAA and A-RSA (Fig. 6M; Table 1). All *Tbx1*$^{+/-}$;*Pax9*$^{+/-}$ embryos examined, however, had some form of 4th PAA-derived defect (Fig. 6N,O; Table 1) with the incidence of IAA being significantly increased compared with *Tbx1*$^{+/-}$ embryos (*P*<0.001). The incidence of perimembranous VSD was also significantly increased (*P*=0.04), but none of the embryos examined displayed outflow tract defects or bicuspid aortic valve, although an abnormal thymus was frequently observed (Fig. S4; Table S3). *Tbx1*$^{+/-}$;*Pax9*$^{+/-}$ embryos at E10.5 were injected intracardially with ink (Fig. 6P-S) and the patency of the developing 4th PAAs was then compared between *Tbx1*$^{+/-}$ and *Tbx1*$^{+/-}$;*Pax9*$^{+/-}$ embryos (Table 2). All *Tbx1*$^{+/-}$ embryos displayed a predominantly hypoplastic 4th PAA defect, with 50% of embryos having a unilateral, and 50% a bilateral, defect. In *Tbx1*$^{+/-}$;*Pax9*$^{+/-}$ embryos, a significant increase in bilateral aplasia of the 4th PAAs (*P*=0.004) was found, but no defects of PAAs 1, 2, 3 or 6 were seen. RNA analysis showed that *Tbx1*, *Pax9*, *Chd7* and *Gbx2* RNA levels were not significantly changed between the respective single heterozygotes and *Tbx1*$^{+/-}$;*Pax9*$^{+/-}$ pharyngeal arches (Fig. 6T-W).

Tbx1 and *Pax9* interact cell autonomously in the pharyngeal endoderm for 4th PAA formation

The presumed site of the *Tbx1-Pax9* interaction is the pharyngeal endoderm, and to demonstrate a cell-autonomous interaction in this tissue, we crossed *Tbx1*^{flox} mice (Xu et al., 2004) with a novel *Pax9Cre* transgenic mouse (Fig. 7A-C). This *Pax9Cre* strain has the *Cre* recombinase gene inserted into the *Pax9*-coding region and effectively results in a *Pax9*-null allele. The *Pax9Cre* allele functions as expected by activating *R26R*^{lacZ} expression specifically in the pharyngeal endoderm from E9.5 to E11.5 (Fig. 7D-G; Fig. S5), and *Pax9Cre*;*Pax9*^{flox} neonates (i.e. *Pax9*-null) die at birth with the typical *Pax9*$^{-/-}$ phenotype (Fig. 7H-Q). To test the specificity of the *Pax9Cre* allele, the pharyngeal arches of *Pax9Cre*;*eYFP* E9.5 embryos (Fig. 8A) were dissociated into single cells and flow-sorted into eYFP-positive and -negative populations. The eYFP-positive population was significantly enriched for *eYFP* and *Pax9* transcripts (Fig. 8B,C). *Tbx1*^{flox} and *Pax9Cre* mice were intercrossed to create *Tbx1*$^{+/flox}$;*Pax9Cre* embryos, which are double heterozygous for each gene but only in the *Pax9* expression domain. A significant reduction in *Tbx1* RNA levels was observed in *eYFP*-positive flow-sorted pharyngeal endoderm cells from conditionally deleted E9.5 mutant embryos compared with *Pax9Cre*;*eYFP* controls (Fig. 8D). Litters from a *Tbx1*$^{+/flox}$ and *Pax9Cre* cross were collected on the day of birth; a significant reduction in the expected number of *Tbx1*$^{+/flox}$;*Pax9Cre* mutants was found (*P*=2.4×10^{-5}; Table S4) and 62.5% of these mutants displayed an arch artery defect (Fig. 8F; Table 1). We then collected embryos (E13.5-E15.5) and analysed them by MRI or μCT, which revealed that 38.5% of mutants presented with an arch artery defect (Fig. 8H; Table 1) and an abnormal thymus (Fig. S4; Table S3). We also collected embryos at E10.5 and injected them intracardially with ink to visualise the PAAs. All *Tbx1*$^{+/flox}$ control embryos analysed had normal PAAs, with all three vessels being patent to ink and of a similar diameter, while the majority of *Tbx1*$^{+/flox}$;*Pax9Cre* mutant embryos presented with some form of 4th PAA defect (Fig. 8J; Table 2).

In summary, our data show that *Pax9* is crucial for cardiovascular development, and when lost the PAAs and outflow tract fail to develop correctly, resulting in postnatal death. The 4th PAAs do not form and

the 3rd PAAs collapse with reduced recruitment from vascular SMC. Our data also demonstrate that *Tbx1* and associated genes are deregulated in *Pax9*-null embryos, and *Tbx1* and *Pax9* function together in the pharyngeal endoderm for 4th PAA morphogenesis.

DISCUSSION
Loss of *Pax9* results in complex cardiovascular defects

Pax9 plays a key role in cardiovascular development, as *Pax9*$^{-/-}$ neonates and embryos display a range of cardiovascular defects. Gene mutations and chromosomal deletions that include *PAX9* have been identified in individuals with cardiovascular abnormalities and other conditions (Table S5), suggesting that *PAX9* has potential importance in human cardiovascular development. Of these, one individual with a 105 kb hemizygous deletion of 14q13 presented with IAA, a hypoplastic aorta, bicuspid aortic valve and a ventricular septal defect (Santen et al., 2012), all of which appear with high penetrance in mouse *Pax9*-null embryos. This small deletion removed only *PAX9*, *NKX2-1* and *NKX2-8*, although deletion of either *Nkx2* gene in mice does not result in any cardiovascular defects (Kimura et al., 1996; Pabst et al., 2003). It is therefore possible that hemizygous deletion of *PAX9* in humans can recapitulate, in part, the mouse knockout phenotype.

Tbx1 and *Pax9* interact in 4th PAA development

Published microarray studies investigating the transcriptome of *Tbx1*-null embryos have implicated *Pax9* as a downstream target of *Tbx1* (Ivins et al., 2005; Liao et al., 2008). Further evidence of crosstalk between *Tbx1* and *Pax9* has been suggested via the interaction of *Ripply3* (Okubo et al., 2011). This protein, which is a Tbx1 repressor, has been shown to prevent Tbx1 activation of luciferase from a *Pax9* promoter construct, and *Pax9* expression in the pharyngeal endoderm is increased in *Ripply3*-null embryos suggesting that *Tbx1* may be upstream of *Pax9*. *Ripply3* levels were not significantly changed in our *Pax9*-null pharyngeal arch transcriptome data, but *Tbx1* levels were significantly reduced, indicating that perhaps *Pax9* and *Tbx1* may function together rather than work in a hierarchal pathway. This is further supported by analysis of *Tbx1* and *Pax9* RNA levels in *Tbx1*$^{+/-}$;*Pax9*$^{+/-}$ embryos, which were not significantly changed compared with levels seen in the single heterozygotes. Further analysis identified that many genes differentially expressed in *Tbx1*-null embryos, or shown to interact with *Tbx1* in mouse models, were also significantly differentially expressed in *Pax9*-null embryos, e.g. *Chd7* and *Gbx2*. Mice heterozygous for *Chd7* have abnormal 4th PAA derivatives and a combined heterozygosity with *Tbx1* results in an increased incidence of 4th PAA defects (Randall et al., 2009). *Gbx2*-null embryos display cardiovascular defects (Byrd and Meyers, 2005), and *Tbx1* and *Gbx2* have also been shown to genetically interact in PAA development (Calmont et al., 2009). Although both these *Tbx1* targets have been demonstrated to interact in the pharyngeal ectoderm, they are also expressed in the pharyngeal endoderm and could therefore interact with *Pax9* either directly or indirectly in this tissue. As our data strongly suggested that *Pax9* may interact with *Tbx1* and its related genes in the morphogenesis of the PAAs, we therefore looked for a genetic interaction between *Tbx1* and *Pax9* in mice. We found that all mice examined (embryos and neonates) double heterozygous for each gene (i.e. *Tbx1*$^{+/-}$;*Pax9*$^{+/-}$) displayed some defect associated with abnormal development of the 4th PAA, most notably IAA-B. Although hypoplasia or absence of the 4th PAAs is a feature in mouse embryos heterozygous for *Tbx1* (Lindsay et al., 2001), this phenotype was significantly more
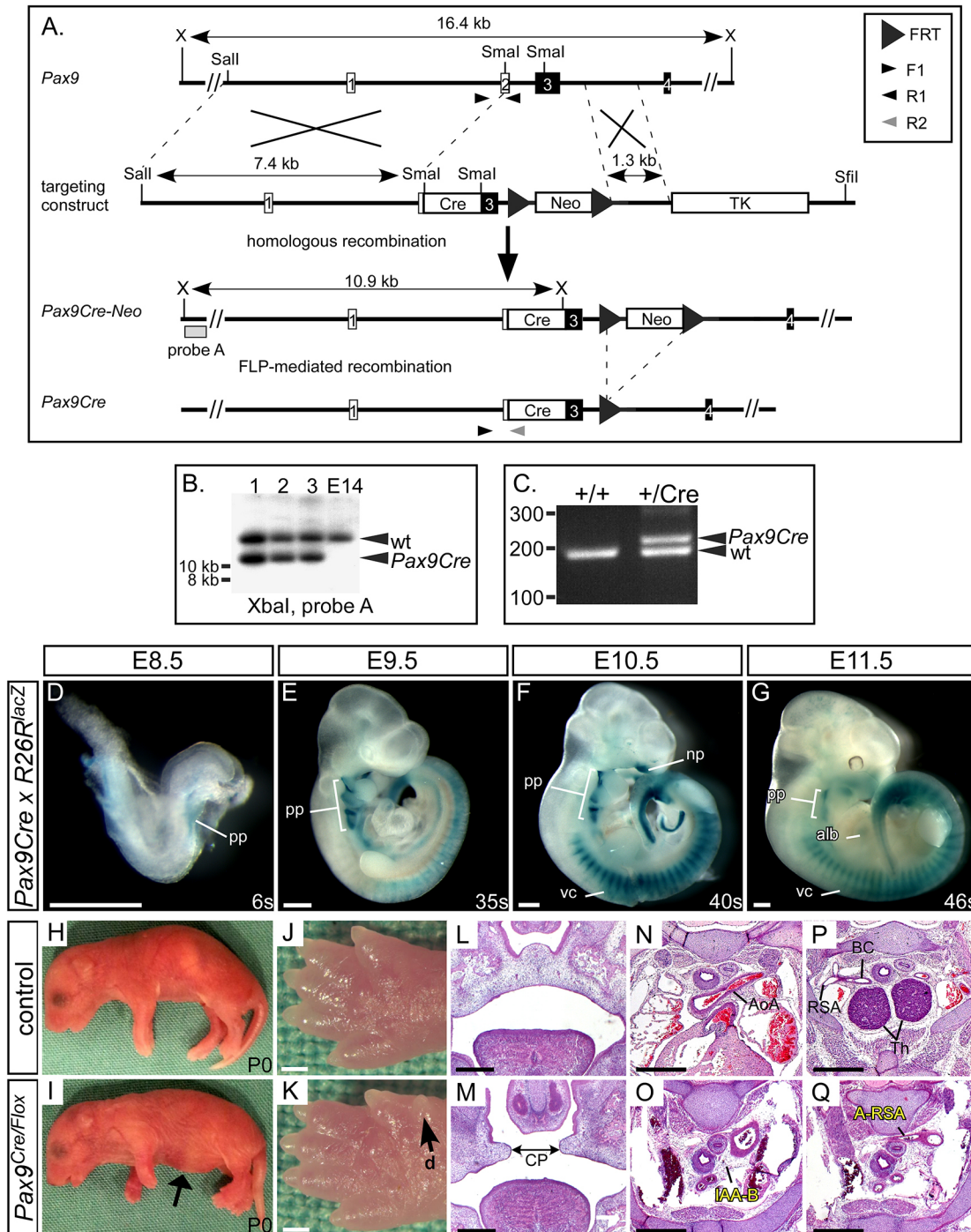
Fig. 7. Generation of the *Pax9Cre* mouse. (A) A *Pax9Cre* targeting vector was created with a *Cre* cassette inserted into the SmaI restriction sites found in exons 2 and 3 of the *Pax9* gene. For transformation, the vector was linearised with SfiI. (B) Correctly targeted ES cells were identified by Southern blotting on XbaI-digested genomic DNA. (C) The derived *Pax9Cre-Neo* mice were crossed with *FLPe*-expressing mice to remove the neomycin cassette and create *Pax9Cre* mice, which were genotyped using the indicated primers. (D-G) *Pax9Cre* mice were mated with *R26R^{lacZ}* reporter mice and embryos were stained with X-Gal at E8.5 (*n*=3), E9.5 (*n*=7), E10.5 (*n*=6) and E11.5 (*n*=5). Positive staining in regions known to express Pax9 was observed (alb, anterior limb bud; np, nasal process; pp, pharyngeal pouch; vc, vertebral column). (H-Q) *Pax9Cre* and *Pax9^{flox/flox}* mice were crossed to create *Pax9^{+/flox}* (control) and *Pax9^{Cre/flox}* (mutant) mice. All *Pax9^{Cre/flox}* neonates died on the day of birth and presented with the typical *Pax9*-null phenotype (*n*=5), including a bloated abdomen (I, arrow) and pre-axial digit duplication (d) in the hind limb (K, arrow). Sections of E14.5-E15.5 embryos (*n*=6) showed cleft palate (CP; M), absent thymus and cardiovascular defects (O,Q). AoA, aortic arch; BC, brachiocephalic; Th, thymus. Somite counts (s) are indicated. Scale bars: 500 µm.

prevalent in *Tbx1^{+/−}*;*Pax9^{+/−}* mice, and much higher than observed in *Tbx1^{+/−}* embryos. It therefore appears that combining one *Pax9*-null allele with one *Tbx1*-null allele exacerbates the *Tbx1^{+/−}* phenotype.

We used our novel *Pax9Cre* mouse to conditionally delete *Tbx1* from the pharyngeal endoderm, while simultaneously creating double haploinsufficiency for the two genes in this tissue. A highly significant reduction in the number of *Tbx1^{+/flox}*;*Pax9Cre* neonates
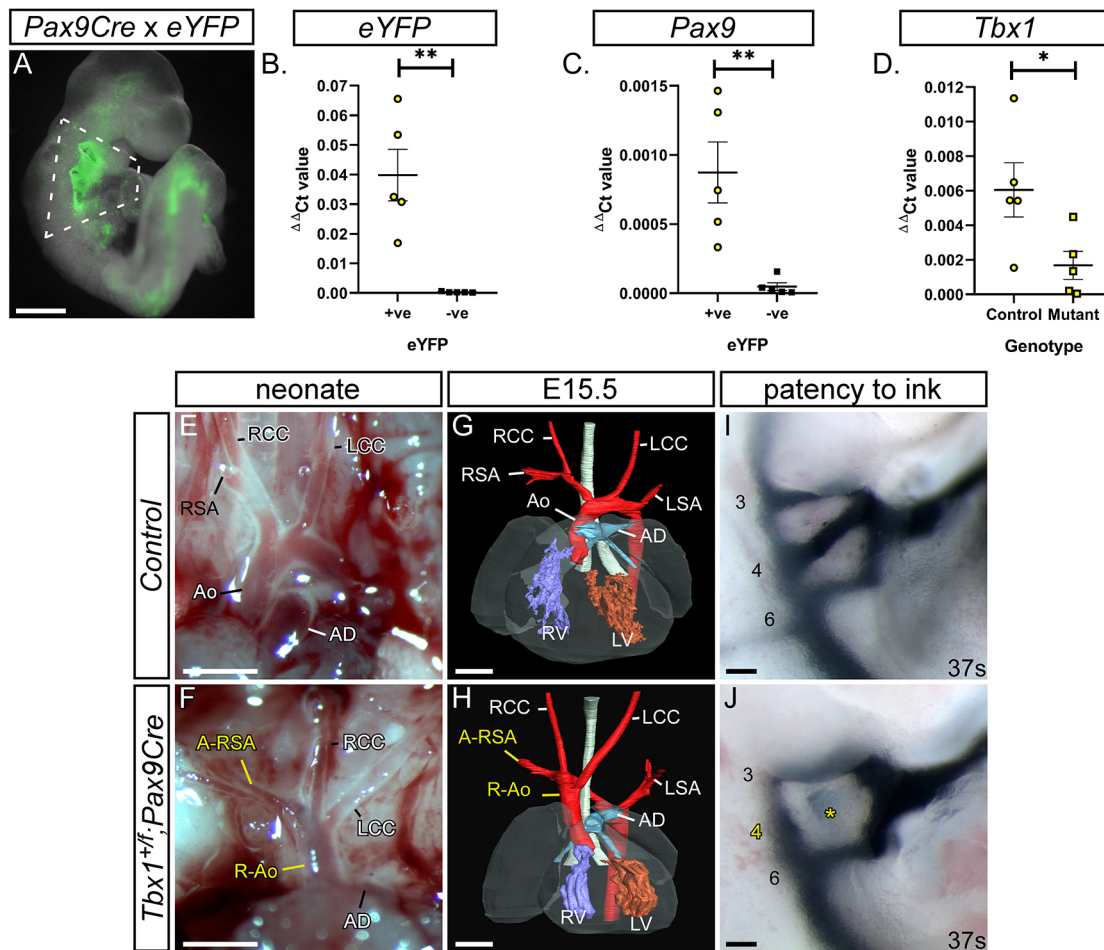
Fig. 8. Conditional deletion of *Tbx1* from the pharyngeal endoderm. (A) *Pax9Cre* drives expression of the eYFP reporter gene in the pharyngeal endoderm at E9.5. Scale bar: 500 μm. (B-D) Flow sorting and qPCR of eYFP-positive and -negative pharyngeal arch cells from *Pax9Cre;eYFP* control and *Tbx1$^{+/flox}$;Pax9Cre* E9.5 embryos (*n*=5 of each; dissected as shown in A). From control embryos, the eYFP-positive cells (yellow circles) were significantly enriched for *eYFP* (B) and *Pax9* (C) compared with eYFP-negative cells (black squares). (D) There was a significant reduction in *Tbx1* levels in *Tbx1$^{+/flox}$;Pax9Cre* (mutant) eYFP-positive cells (yellow squares) compared with controls (yellow circles). *$P<0.05$, **$P<0.01$ (two-tailed unpaired *t*-test). (E-J) Cardiovascular defects in *Tbx1$^{+/flox}$;Pax9Cre* mice. (E,F) Neonates were collected shortly after birth and the aortic arch arteries examined. (E) Control neonates (*n*=39 wild-type, *n*=43 *Pax9Cre* and *n*=33 *Tbx1$^{+/flox}$*) all had normal arch arteries. (F) *Tbx1$^{+/flox}$;Pax9Cre* mutants (*n*=8) had cardiovascular defects such as a right-sided aorta (R-Ao) and A-RSA. Scale bars: 1 mm. (G,H) Embryos at E13.5-E15.5 were analysed by imaging (*n*=26 mutants). (G) Control embryo with normal cardiovascular system. (H) In the mutant there is a vascular ring formed by a R-Ao and an A-RSA. Scale bars: 500 μm. (I,J) Embryos collected at E10.5 (36-43 s) were injected intra-cardially with ink. (I) In *Tbx1$^{+/flox}$* control embryos (*n*=15), PAAs 3-6 were patent to ink. (J) In *Tbx1$^{+/flox}$;Pax9Cre* mutant embryos (*n*=17), the 4th PAA was frequently absent (asterisk). Somite counts (s) are indicated. Scale bars: 100 μm. Ao, aorta; AD, arterial duct; LCC, left common carotid artery; LSA, left subclavian artery; LV, left ventricle; RCC, right common carotid artery; RSA, right subclavian artery; RV, right ventricle. The somite numbers given in the legend reflect the range analysed for the whole study. The figure contains representative images only.

born was observed, indicating that heterozygous loss of *Tbx1* and *Pax9* from the pharyngeal endoderm has a major impact on postnatal survival, with almost two-thirds of the recovered neonates examined having identifiable cardiovascular defects. A similar proportion of affected mutants was found at foetal stages. A vascular ring structure was observed in *Tbx1$^{+/flox}$;Pax9Cre* mutants (Fig. 8H), similar to that described in *Lgdel/+* mice, which are chromosomally engineered to be hemizygous for *Tbx1* (Merscher et al., 2001), and also in *Six1;Eya1* mutant embryos (Guo et al., 2011a). *Eya1* was significantly reduced in *Pax9*-null pharyngeal arch tissue. When embryos were examined at mid-embryogenesis, however, we found that almost all displayed 4th PAA defects. When compared with our *Tbx1$^{+/–}$;Pax9$^{+/–}$* embryo data it was apparent that there was no significant difference in the incidence of bilateral 4th PAA defects between *Tbx1$^{+/flox}$;Pax9Cre* and *Tbx1$^{+/–}$;Pax9$^{+/–}$* embryos. This indicates that the conditional heterozygous deletion

of *Tbx1* from the pharyngeal endoderm, in the context of *Pax9* heterozygosity, has the same effect on 4th PAA morphogenesis as seen in the global *Tbx1$^{+/–}$;Pax9$^{+/–}$* embryos at E10.5. Although the ink injection data from *Tbx1$^{+/flox}$;Pax9Cre* embryos matches that seen in *Tbx1$^{+/–}$;Pax9$^{+/–}$* embryos, and shows that heterozygous loss of *Tbx1* from the pharyngeal endoderm severely affects PAA morphogenesis, there is a discrepancy in the cardiovascular phenotype observed at foetal and neonatal stages that does not reflect that seen at mid-embryogenesis, nor that observed in *Tbx1$^{+/–}$;Pax9$^{+/–}$* embryos. It is well documented, however, that the *Tbx1$^{+/–}$* 4th PAA phenotype does recover during development (see Table S6). It therefore appears that a conditional deletion of *Tbx1* from the pharyngeal endoderm in the context of *Pax9* haploinsufficiency replicates the *Tbx1* heterozygous arch artery phenotype in terms of a highly penetrant 4th PAA defect at mid-embryogenesis that partially recovers by the foetal stage. Our data,

however, do raise the question of whether we are seeing the effect of a pharyngeal endoderm-specific loss of *Tbx1* with *Pax9Cre* or a genetic interaction occurring between *Tbx1* and *Pax9* in the pharyngeal endoderm? Conditional deletion experiments have been performed in transgenic mice to identify the role of *Tbx1* in specific tissues and have examined the effect of *Tbx1* heterozygosity in the pharyngeal mesoderm and/or epithelium for 4th PAA development (see Table S7). When compared, our data clearly show that the 4th PAA phenotype is much more penetrant than that seen in embryos only heterozygous for *Tbx1* in the pharyngeal epithelia. We therefore conclude that we are showing a strong genetic and cell-autonomous interaction between *Tbx1* and *Pax9* within the pharyngeal endoderm that impacts on 4th PAA morphogenesis. Moreover, and in support of a phenotype extending beyond what is expected from a *Tbx1* heterozygous phenotype, our *Tbx1^{flox}; Pax9Cre* mice display a high incidence of perinatal lethality, a feature not previously described in *Tbx1^{+/-}* mice. Interestingly, the homozygous deletion of *Tbx1* from the pharyngeal endoderm using *Sox17Cre* mice resulted in pharyngeal arch aplasia but not in a common arterial trunk, although IAA was observed (Jackson et al., 2014). This phenotype is similar to that seen in our *Tbx1;Pax9* mutants but is distinct from either *Tbx1* and *Pax9* constitutive null mutants.

Pax9 signalling from the pharyngeal endoderm is required for 3rd PAA maintenance

The mammalian PAAs develop symmetrically in a cranial to caudal sequence, and then subsequently remodel to form the typical asymmetric aortic arch artery system seen in the adult (Bamforth et al., 2013; Hiruma et al., 2002). In normal PAA development, the 1st artery forms first, followed by the 2nd, but these two vessels rapidly remodel and contribute to capillary beds and the mandibular and hyoid arteries. In some *Pax9^{-/-}* embryos, these vessels aberrantly persisted into E10.5 and E11.5, and may contribute to the anomalous arrangement of the aortic arch arteries when the 3rd PAAs collapse. In normal development, the 3rd PAAs will form part of the common and proximal internal carotid arteries, which elongate as the embryo grows. The carotid duct involutes and the dorsal aorta anterior to this segment will form the distal internal carotid artery, with the external carotid artery derived from the proximal parts of the 1st and 2nd PAA (Hiruma et al., 2002). The persistence of the 1st and/or 2nd PAAs in *Pax9^{-/-}* embryos, coupled with the failure of the 3rd PAAs to be maintained and the carotid duct to involute, results in the external carotid arteries rising directly from the aorta, and the internal carotid arteries from the anterior dorsal aortae. This phenomenon has been described clinically (Roberts and Gerald, 1978). Although reduced numbers of NCCs were found in the caudal pharyngeal arches at E10.5, migration, apoptosis or proliferation of NCCs did not appear to be impaired in *Pax9*-null embryos. It is well recognised that NCCs differentiate into the SMCs that are important for the stabilisation of the remodelled PAAs (Hutson and Kirby, 2003) and it is likely that the failure of SMCs to envelop the 3rd PAAs in *Pax9*-null embryos results in the collapse of this vessel. This has also been described in *Hoxa3*-null embryos (Kameda, 2009) and reduced NCC migration in genetic mouse and surgical chick models also leads to defects of the 3rd PAAs (Bradshaw et al., 2009; Epstein et al., 2000; Franz, 1989; Nishibatake et al., 1987). We were unable to look for a similar occurrence in the 4th PAAs, as this fails to form in the majority of *Pax9*-null embryos. Signalling between the pharyngeal endoderm and NCC does occur (Graham et al., 2005) so it is therefore possible that signals emanating from the pharyngeal endoderm under Pax9

control are necessary to influence the differentiation of NCCs into SMCs; without these signals, the 3rd PAAs are not supported during the remodelling phase of arch artery development and they collapse. The top two GSEA pathways identified from the RNA-seq data were 'extracellular matrix organisation' and 'axon guidance', and these could be relevant for a NCC-derived phenotype, particularly as the extracellular matrix is known to be crucial for the migration of NCCs (Henderson and Copp, 1997; Perris and Perissinotto, 2000) and the slit, ephrin, semaphorin and plexin genes listed under 'axon guidance' are usually associated with NCC expression or migration in cardiovascular development (Epstein et al., 2015; Kirby and Hutson, 2010; Sun et al., 2018). There is, however, an alternative explanation for the collapse of the 3rd PAAs. Haemodynamic force plays a major role in artery development (Culver and Dickinson, 2010; Yashiro et al., 2007), so it is possible that the 3rd PAA defect is a consequence of increased blood flow to the persistent 1st/2nd PAAs, which prevents sufficient blood flow to the 3rd PAAs, resulting in impairment of flow-induced arteriogenesis. This may also be an explanation for the failure of the 4th PAAs to form. A reduced haemodynamic force would also explain the reduction in SMC recruitment as this is also dependent on blood flow (Padget et al., 2019). Although endothelial cells were present within the 4th pharyngeal arch of *Pax9*-null embryos, they apparently failed to condense into tubes, a feature that has also been described in both *Tbx1*-null and *Gbx2*-null embryos (Byrd and Meyers, 2005; Calmont et al., 2009).

The double outlet right ventricle phenotype observed at E15.5 in *Pax9*-null embryos probably arises from the marked outflow tract rotation defect due to a change in the aortic to pulmonary valve axis angle (Bostrom and Hutchins, 1988; Lomonico et al., 1986), which is also observed in *Pax3* and *Pitx2c* mutant hearts (Bajolle et al., 2006).

In summary, Pax9 expression in the pharyngeal endoderm has regional (anterior/posterior) roles in regulating the morphogenesis of the PAAs (Fig. 9). In the 3rd pharyngeal arch, Pax9 is important for controlling NCC differentiation into the SMCs that support the remodelling vessel, whereas in the 4th pharyngeal arch endoderm, the interaction of *Pax9* with *Tbx1* and its targets is crucial for the formation of the 4th PAAs.

MATERIALS AND METHODS
Mice

Generation of *Pax9Cre* mice
The *Pax9Cre* targeting construct was designed to replace a 1.06 kb section of the *Pax9* gene, spanning the second half of exon two, containing the start codon, and the first half of the 3rd exon, containing the paired box and octapeptide motif, with a promoterless *Cre* recombinase gene preceded by a consensus Kozak sequence, in the pPNT4 targeting vector (Conrad et al., 2003), using standard molecular biology methods (Fig. 7A). The 1.3 kb right homology arm, generated as previously described (Kist et al., 2005), was inserted between the FRT-flanked PGK-Neomycin cassette and the HSV-Thymidine Kinase cassette of pPNT4. The unwanted loxP site of pPNT4 was removed by XbaI partial digestion, followed by Klenow treatment and re-ligation. The left homology arm was generated as a 7.4 kb SalI to SmaI fragment of the *Pax9* genomic region that included exon 1 and the first half of the second exon, and was inserted 5′ of the *Cre* recombinase
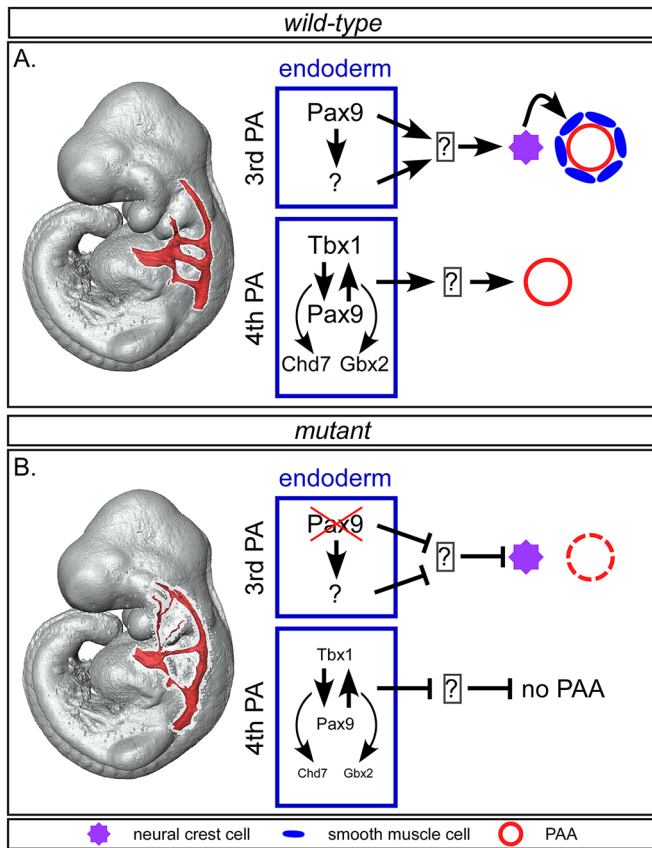
Fig. 9. Proposed model for role of Pax9-mediated signalling during pharyngeal arch artery development. (A) In wild-type embryos, *Pax9* expression in the 3rd pharyngeal arch endoderm induces neural crest cells (NCCs), either directly or indirectly, to differentiate into the SMCs that form around the endothelium of the remodelling 3rd PAAs. In the 4th arch endoderm, *Tbx1* and *Pax9* function together to, most likely indirectly, control formation of the 4th PAAs, potentially through collaboration with *Chd7* and *Gbx2*. (B) In *Pax9*-deficient embryos, signals from the 3rd pharyngeal arch endoderm are compromised and NCC differentiation into SMCs is impaired, resulting in the collapse of the 3rd PAAs by E11.5. In *Tbx1-Pax9* double heterozygous embryos, reduced levels of *Tbx1* and *Pax9* in the 4th pharyngeal arch endoderm are insufficient to allow the 4th PAAs to form.

gene. The targeting vector was linearized with SfiI and mouse ES cells were targeted and selected as previously described (Kearns et al., 2013). Southern blot analysis was performed according to standard methods following XbaI digest of genomic DNA. An external southern probe was used to verify integration of the targeting cassette in the 5′ region (Fig. 7B) and PCR was used to validate integration of the 3′ region (not shown). The FRT-flanked PGK-neomycin cassette was removed by crossing the derived *Pax9Cre-Neo* mice with *FLPe* mice (Dymecki, 1996) to create *Pax9Cre* mice, which were then backcrossed to strain C57Bl/6J for over six generations. Genotyping by multiplex PCR [primers: F1-ACTCAAGCCTCTTTCAGCCC (common), R1-TTGTTCTCACTGAGCCGGCCTGT (Pax9 exon 2) and R2-GTTGC-ATCGACCGGTAATGC (Cre)] were used to simultaneously identify the wild-type and *Pax9Cre* alleles (Fig. 7C).

Breeding
Male and female mice were mated and the detection of a vaginal plug the next morning considered to be E0.5. Pregnant females were culled on the required day and embryos collected. Embryos at E9.5-E11.5 were staged by somite counting.

Imaging
Magnetic resonance imaging (MRI) was performed using a 9.4T MR system (Varian, US) as previously described (Bamforth et al., 2012; Schneider et al.,

2004) on embryos at E15.5. High Resolution Episcopic Microscopy (HREM) and micro-computed tomography (μCT) techniques have been described in detail elsewhere (Degenhardt et al., 2010; Geyer et al., 2009). All MRI, HREM and μCT images were converted into a volume dataset and segmented using Amira software (Thermo Fisher Scientific) to create 2- and 3-dimensional (3D) images. Structures were manually outlined using the label field function of Amira and surface rendered to produce the 3D images. Intra-cardiac ink injections were performed as described previously (Calmont et al., 2009). Aorta measurements were taken from the region just proximal to the point at which the ascending aorta becomes the aortic arch. Haematoxylin and Eosin staining, X-gal staining and *Pax9* whole-mount *in situ* hybridisation were performed using standard techniques. mRNA expression on sections was examined by *in situ* hybridisation using RNAscope Multiplex Fluorescent v2 Assay (Advanced Cell Diagnostics) following the manufacturer's instructions. Probe details given in Table S8. For proliferation assays, BrdU (Sigma-Aldrich) dissolved in PBS was administered by intraperitoneal injection at a dose of 50 mg/kg to pregnant dams 1 h before embryo collection. Immunohistochemistry was performed using standard techniques (antibody details are in Table S8) on paraformaldehyde-fixed embryo sections and fluorescently imaged on an Axioimager (Zeiss). To assess an apoptotic index within the pharyngeal arches, control and $Pax9^{-/-}$ embryos at E9.5 (n=3 per genotype; 24-28 somites) and E10.5 (n=3 per genotype; 30-35 somites) were examined following immunostaining with the anti-caspase 3 antibody. To assess a proliferative index within the NCC in the pharyngeal arches, control and $Pax9^{-/-}$ embryos expressing *Wnt1Cre* activated eYFP at E9.5 (n=3 per genotype; 23-28 somites) and E10.5 (n≥4 for each genotype; 31-39 somites) were examined following immunostaining using anti-BrdU and anti-GFP antibodies. All positively stained and DAPI-positive cells within the pharyngeal arches were counted and the ratio of positively stained cells over the total number of cells calculated. The average number of NCCs within the caudal pharyngeal arches was calculated at E9.5 (n=3 per genotype, 23-28 somites) and E10.5 (n=4 per genotype, 32-34 somites). For all cell counting experiments, at least three sections per embryo were assessed.

Transcriptome analysis
Wild-type ($Pax9^{+/+}$) and *Pax9*-null ($Pax9^{-/-}$) embryos at E9.5 (n=3 of each genotype, stage-matched for 26-27 somites) were collected in ice-cold DEPC-PBS and the pharyngeal region, from the junction between the first and second pharyngeal arch to the base of the heart, was dissected free in RNA*later* (Sigma-Aldrich). Genotypes were identified by PCR from the embryo tails and/or yolk sac material. Total RNA was extracted using the QIAGEN Plus Micro kit with genomic DNA Eliminator columns, and total RNA eluted in 30 μl RNase-free water. RNA concentration and purity were assessed by NanoDrop spectrophotometry and Agilent Bioanalyzer with all samples producing a RIN of 10. Genomic DNA contamination was excluded by PCR for intronic regions (sensitivity 5 pg/μl). To confirm that the correct genotypes were processed, cDNA was made from 100 ng total RNA and a qPCR for *Pax9* performed (Fig. 5B). The total RNA samples were shipped on dry-ice to EMBLM-GeneCore for RNA-seq first-strand specific library preparation using Illumina TruSeq, and 100 bp paired end reads were generated from an Illumina HiSeq 2000 Sequencer. Quality control by FastQC suggested a small amount of adaptor contamination in each sample, so raw reads were trimmed of adaptor sequence with Trimmomatic (Bolger et al., 2014). Reads shorter than 36 bp after trimming were discarded, and reads whose pair had been discarded were also removed. Trimmed reads were further filtered to keep only uniquely aligned and non-redundant reads to remove a vast majority of pseudogenes caused by multi-mapping. In addition, to avoid bias due to imbalanced library sizes among conditions, all samples were sub-sampled towards the smallest sample (mt-663_1). The resulting reads were aligned to the Mouse Genome (Ensembl release 81, GRCm38) using the splice aware read aligner STAR 2 (star-2.5.2a-0, 20/01/2017) (Dobin et al., 2013). Finally, aligned reads were assigned to Ensembl genes using featureCounts (Liao et al., 2014) with default parameters. These count tables were imported into R and analysed using the package LIMMA (Ritchie et al., 2015) and voom function from Bioconductor (Gentleman et al., 2004). A gene set enrichment analysis tool (Subramanian et al., 2005) was used to predict signalling pathways that were

affected when gene expression in the wild-type and the *Pax9* mutant samples was compared. All resulting pathways were filtered for a familywise-error rate ($P<0.001$) to correct for multiple hypotheses testing.

Flow cytometry

The pharyngeal arch region of E9.5 *Pax9Cre;eYFP* control ($n=5$; 23-27 somites) and mutant *Tbx1$^{+/flox}$;Pax9Cre;eYFP* ($n=5$; 24-29 somites) embryos was dissected free as described above and dissociated to single cells with Accumax (eBioscience) by incubating at 37°C for 30 min. The reaction was stopped by the addition of 10% foetal calf serum (FCS), and cells were washed in PBS and resuspended in 10% FCS. Cells were stained with propidium iodide. Fluorescence-activated cell sorting was performed on a Becton Dickinson FACS Aria II using a 100 μm nozzle and a sheath pressure of 20 psi. Single cells were gated using FSC-A versus SSC-A followed by FSC-A versus FSC-H and FSC-A versus SSC-W to remove any doublets. Live single cells were gated using propidium iodide versus FSC-A, and this population was finally gated on eYFP-positive and -negative cells and sorted into collection tubes.

Quantitative real-time RT-PCR (qPCR)

RNA, from either dissociated pharyngeal arch cells or flow-sorted cells, was extracted using Trizol reagent (Invitrogen) combined with a Purelink RNA Mini Kit (Ambion) and on-column DNase1 treatment. RNA was eluted with 30 μl RNase-free water. Total RNA was converted to cDNA using a High-Capacity cDNA Reverse transcription kit (Applied Biosystems) and random hexamers. qPCR was performed using SYBR Green JumpStart Taq ReadyMix (Sigma-Aldrich) using the primers listed in Table S9. All qPCR reactions were performed in triplicate on a QuantStudio 7 Real-Time PCR System (Thermo Fisher Scientific). Data were analysed using the comparative Ct method (Schmittgen and Livak, 2008).

Statistical analysis

A chi-squared test was used to compare genotype frequencies of litters, and Pearson's chi-squared test for associations was used to compare defect frequencies between the different genotypes. For analysis of qPCR data, aorta measurements and cell counts, datasets were tested for variance using the Shapiro-Wilk test (Prism 8.01 software, GraphPad). Two-tailed unpaired *t*-tests were performed on normally distributed data, and a two-tailed Mann–Whitney *U* non-parametric test was used for not normally distributed data. One-way ANOVA with Tukey's multiple comparison test was used to analyse qPCR data from four embryo genotypes. A hypergeometric distribution test was used to calculate a *P*-value for observing an overlap between two gene lists in R. Groups were considered significantly different when $P<0.05$ or $P\leq0.1$ for RNA-seq data. No statistical methods were used to predetermine sample size, which were chosen based on previous experience to obtain statistical significance and reproducibility. No data points were excluded and all data collected from each individual experiment were used for analysis.

Competing interests

The authors declare no competing or financial interests.

Author contributions

Conceptualization: H.M.P., S.D.B.; Methodology: K.S., T.B., M.N., R.M., R.K., H.P., S.D.B.; Validation: S.D.B.; Formal analysis: A.I.K., S.J.C., S.D.B.; Investigation: C.A.S., W.M.S.Q., J.A.B.-L., R.R.K., C.O., R.S., S.M., R.D., T.B., J.E.S., T.J.M., R.K., S.D.B.; Resources: H.M.P., K.S., T.B., M.N., J.E.S., T.J.M., R.M., R.K., H.P., S.D.B.; Writing - original draft: S.D.B.; Writing - review & editing: H.M.P., R.K., H.P.; Visualization: A.I.K., S.D.B.; Supervision: H.M.P., R.K., H.P., S.D.B.; Project administration: H.M.P., S.D.B.; Funding acquisition: S.D.B.

Data availability

The RNA-seq data have been deposited in GEO under accession number GSE128087.

Supplementary information

Supplementary information available online at
http://dev.biologists.org/lookup/doi/10.1242/dev.177618.supplemental

References

Aggarwal, V. S. and Morrow, B. E. (2008). Genetic modifiers of the physical malformations in velo-cardio-facial syndrome/DiGeorge syndrome. *Dev. Disabil. Res. Rev.* **14**, 19-25. doi:10.1002/ddrr.4

Bajolle, F., Zaffran, S., Kelly, R. G., Hadchouel, J., Bonnet, D., Brown, N. A. and Buckingham, M. E. (2006). Rotation of the myocardial wall of the outflow tract is implicated in the normal positioning of the great arteries. *Circ. Res.* **98**, 421-428. doi:10.1161/01.RES.0000202800.85341.6e

Bamforth, S. D., Schneider, J. E. and Bhattacharya, S. (2012). High-throughput analysis of mouse embryos by magnetic resonance imaging. *Cold Spring Harb. Protoc.* **2012**, 93-101. doi:10.1101/pdb.prot067538

Bamforth, S. D., Chaudhry, B., Bennett, M., Wilson, R., Mohun, T. J., Van Mierop, L. H. S., Henderson, D. J. and Anderson, R. H. (2013). Clarification of the identity of the mammalian fifth pharyngeal arch artery. *Clin. Anat.* **26**, 173-182. doi:10.1002/ca.22101

Bolger, A. M., Lohse, M. and Usadel, B. (2014). Trimmomatic: a flexible trimmer for Illumina sequence data. *Bioinformatics* **30**, 2114-2120. doi:10.1093/bioinformatics/btu170

Bostrom, M. P. and Hutchins, G. M. (1988). Arrested rotation of the outflow tract may explain double-outlet right ventricle. *Circulation* **77**, 1258-1265. doi:10.1161/01.CIR.77.6.1258

Boudjemline, Y., Fermont, L., Le Bidois, J., Lyonnet, S., Sidi, D. and Bonnet, D. (2001). Prevalence of 22q11 deletion in fetuses with conotruncal cardiac defects: a 6-year prospective study. *J. Pediatr.* **138**, 520-524. doi:10.1067/mpd.2001.112174

Bradshaw, L., Chaudhry, B., Hildreth, V., Webb, S. and Henderson, D. J. (2009). Dual role for neural crest cells during outflow tract septation in the neural crest-deficient mutant Splotch(2H). *J. Anat.* **214**, 245-257. doi:10.1111/j.1469-7580.2008.01028.x

Byrd, N. A. and Meyers, E. N. (2005). Loss of Gbx2 results in neural crest cell patterning and pharyngeal arch artery defects in the mouse embryo. *Dev. Biol.* **284**, 233-245. doi:10.1016/j.ydbio.2005.05.023

Calmont, A., Ivins, S., Van Bueren, K. L., Papangeli, I., Kyriakopoulou, V., Andrews, W. D., Martin, J. F., Moon, A. M., Illingworth, E. A., Basson, M. A. et al. (2009). Tbx1 controls cardiac neural crest cell migration during arch artery development by regulating Gbx2 expression in the pharyngeal ectoderm. *Development* **136**, 3173-3183. doi:10.1242/dev.028902

Chi, N. and Epstein, J. A. (2002). Getting your Pax straight: Pax proteins in development and disease. *Trends Genet.* **18**, 41-47. doi:10.1016/S0168-9525(01)02594-X

Conrad, M., Brielmeier, M., Wurst, W. and Bornkamm, G. W. (2003). Optimized vector for conditional gene targeting in mouse embryonic stem cells. *BioTechniques* **34**, 1136-1138, 1140. doi:10.2144/03346bm03

Culver, J. C. and Dickinson, M. E. (2010). The effects of hemodynamic force on embryonic development. *Microcirculation* **17**, 164-178. doi:10.1111/j.1549-8719.2010.00025.x

Danielian, P. S., Muccino, D., Rowitch, D. H., Michael, S. K. and McMahon, A. P. (1998). Modification of gene activity in mouse embryos in utero by a tamoxifen-inducible form of Cre recombinase. *Curr. Biol.* **8**, 1323-1326. doi:10.1016/S0960-9822(07)00562-3

Degenhardt, K., Wright, A. C., Horng, D., Padmanabhan, A. and Epstein, J. A. (2010). Rapid 3D phenotyping of cardiovascular development in mouse embryos by micro-CT with iodine staining. *Circ. Cardiovasc. Imaging* **3**, 314-322. doi:10.1161/CIRCIMAGING.109.918482

Dobin, A., Davis, C. A., Schlesinger, F., Drenkow, J., Zaleski, C., Jha, S., Batut, P., Chaisson, M. and Gingeras, T. R. (2013). STAR: ultrafast universal RNA-seq aligner. *Bioinformatics* **29**, 15-21. doi:10.1093/bioinformatics/bts635

Dymecki, S. M. (1996). Flp recombinase promotes site-specific DNA recombination in embryonic stem cells and transgenic mice. *Proc. Natl. Acad. Sci. USA* **93**, 6191-6196. doi:10.1073/pnas.93.12.6191
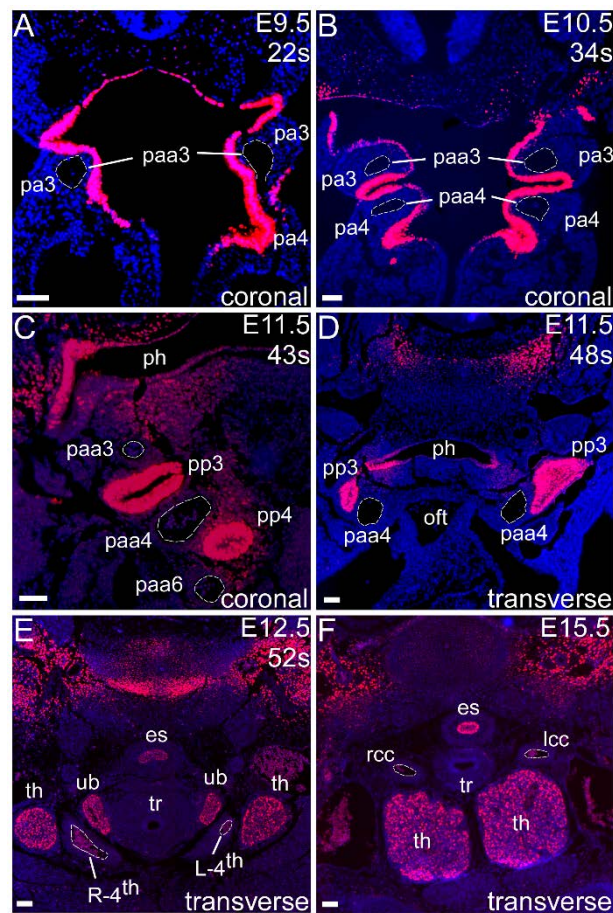
DEVELOPMENT

Epstein, J. A., Li, J., Lang, D., Chen, F., Brown, C. B., Jin, F., Lu, M. M., Thomas, M., Liu, E., Wessels, A. et al. (2000). Migration of cardiac neural crest cells in Splotch embryos. *Development* **127**, 1869-1878.

Epstein, J. A., Aghajanian, H. and Singh, M. K. (2015). Semaphorin signaling in cardiovascular development. *Cell Metab.* **21**, 163-173. doi:10.1016/j.cmet.2014. 12.015

Franz, T. (1989). Persistent truncus arteriosus in the Splotch mutant mouse. *Anat. Embryol.* **180**, 457-464. doi:10.1007/BF00305120

Gentleman, R. C., Carey, V. J., Bates, D. M., Bolstad, B., Dettling, M., Dudoit, S., Ellis, B., Gautier, L., Ge, Y., Gentry, J. et al. (2004). Bioconductor: open software development for computational biology and bioinformatics. *Genome Biol.* **5**, R80. doi:10.1186/gb-2004-5-10-r80

Geyer, S. H., Mohun, T. J. and Weninger, W. J. (2009). Visualizing vertebrate embryos with episcopic 3D imaging techniques. *Sci. World J.* **9**, 1423-1437. doi:10.1100/tsw.2009.154

Graham, A. (2003). Development of the pharyngeal arches. *Am. J. Med. Genet. A* **119A**, 251-256. doi:10.1002/ajmg.a.10980

Graham, A., Okabe, M. and Quinlan, R. (2005). The role of the endoderm in the development and evolution of the pharyngeal arches. *J. Anat.* **207**, 479-487. doi:10.1111/j.1469-7580.2005.00472.x

Guo, C., Sun, Y., Zhou, B., Adam, R. M., Li, X. K., Pu, W. T., Morrow, B. E., Moon, A. and Li, X. (2011a). A Tbx1-Six1/Eya1-Fgf8 genetic pathway controls mammalian cardiovascular and craniofacial morphogenesis. *J. Clin. Invest.* **121**, 1585-1595. doi:10.1172/JCI44630

Guo, T., McDonald-McGinn, D., Blonska, A., Shanske, A., Bassett, A. S., Chow, E., Bowser, M., Sheridan, M., Beemer, F., Devriendt, K. et al. (2011b). Genotype and cardiovascular phenotype correlations with TBX1 in 1,022 velo-cardio-facial/DiGeorge/22q11.2 deletion syndrome patients. *Hum. Mutat.* **32**, 1278-1289. doi:10.1002/humu.21568

Henderson, D. J. and Copp, A. J. (1997). Role of the extracellular matrix in neural crest cell migration. *J. Anat.* **191**, 507-515. doi:10.1046/j.1469-7580.1997. 19140507.x

Hiruma, T., Nakajima, Y. and Nakamura, H. (2002). Development of pharyngeal arch arteries in early mouse embryo. *J. Anat.* **201**, 15-29. doi:10.1046/j.1469-7580.2002.00071.x

Hutson, M. R. and Kirby, M. L. (2003). Neural crest and cardiovascular development: a 20-year perspective. *Birth Defects Res. C Embryo Today* **69**, 2-13. doi:10.1002/bdrc.10002

Ivins, S., Lammerts van Beuren, K., Roberts, C., James, C., Lindsay, E., Baldini, A., Ataliotis, P. and Scambler, P. J. (2005). Microarray analysis detects differentially expressed genes in the pharyngeal region of mice lacking Tbx1. *Dev. Biol.* **285**, 554-569. doi:10.1016/j.ydbio.2005.06.026

Jackson, A., Kasah, S., Mansour, S. L., Morrow, B. and Basson, M. A. (2014). Endoderm-specific deletion of Tbx1 reveals an FGF-independent role for Tbx1 in pharyngeal apparatus morphogenesis. *Dev. Dyn.* **243**, 1143-1151. doi:10.1002/dvdy.24147

Jerome, L. A. and Papaioannou, V. E. (2001). DiGeorge syndrome phenotype in mice mutant for the T-box gene, Tbx1. *Nat. Genet.* **27**, 286-291. doi:10.1038/85845

Kameda, Y. (2009). Hoxa3 and signaling molecules involved in aortic arch patterning and remodeling. *Cell Tissue Res.* **336**, 165-178. doi:10.1007/s00441-009-0760-7

Kearns, N. A., Genga, R. M. J., Ziller, M., Kapinas, K., Peters, H., Brehm, M. A., Meissner, A. and Maehr, R. (2013). Generation of organized anterior foregut epithelia from pluripotent stem cells using small molecules. *Stem Cell Res.* **11**, 1003-1012. doi:10.1016/j.scr.2013.06.007

Kimura, S., Hara, Y., Pineau, T., Fernandez-Salguero, P., Fox, C. H., Ward, J. M. and Gonzalez, F. J. (1996). The T/ebp null mouse: thyroid-specific enhancer-binding protein is essential for the organogenesis of the thyroid, lung, ventral forebrain, and pituitary. *Genes Dev.* **10**, 60-69. doi:10.1101/gad.10.1.60

Kirby, M. L. and Hutson, M. R. (2010). Factors controlling cardiac neural crest cell migration. *Cell Adh. Migr.* **4**, 609-621. doi:10.4161/cam.4.4.13489

Kist, R., Watson, M., Wang, X., Cairns, P., Miles, C., Reid, D. J. and Peters, H. (2005). Reduction of Pax9 gene dosage in an allelic series of mouse mutants causes hypodontia and oligodontia. *Hum. Mol. Genet.* **14**, 3605-3617. doi:10. 1093/hmg/ddi388

Kist, R., Greally, E. and Peters, H. (2007). Derivation of a mouse model for conditional inactivation of Pax9. *Genesis* **45**, 460-464. doi:10.1002/dvg.20295

Lewin, M. B., Lindsay, E. A., Jurecic, V., Goytia, V., Towbin, J. A. and Baldini, A. (1997). A genetic etiology for interruption of the aortic arch type B. *Am. J. Cardiol.* **80**, 493-497. doi:10.1016/S0002-9149(97)00401-3

Liao, J., Aggarwal, V. S., Nowotschin, S., Bondarev, A., Lipner, S. and Morrow, B. E. (2008). Identification of downstream genetic pathways of Tbx1 in the second heart field. *Dev. Biol.* **316**, 524-537. doi:10.1016/j.ydbio.2008.01.037

Liao, Y., Smyth, G. K. and Shi, W. (2014). featureCounts: an efficient general purpose program for assigning sequence reads to genomic features. *Bioinformatics* **30**, 923-930. doi:10.1093/bioinformatics/btt656

Lindsay, E. A., Vitelli, F., Su, H., Morishima, M., Huynh, T., Pramparo, T., Jurecic, V., Ogunrinu, G., Sutherland, H. F., Scambler, P. J. et al. (2001). Tbx1 haploinsufficiency in the DiGeorge syndrome region causes aortic arch defects in mice. *Nature* **410**, 97-101. doi:10.1038/35065105

Lomonico, M. P., Moore, G. W. and Hutchins, G. M. (1986). Rotation of the junction of the outflow tract and great arteries in the embryonic human heart. *Anat. Rec.* **216**, 544-549. doi:10.1002/ar.1092160412

Mansouri, A., Hallonet, M. and Gruss, P. (1996). Pax genes and their roles in cell differentiation and development. *Curr. Opin. Cell Biol.* **8**, 851-857. doi:10.1016/S0955-0674(96)80087-1

Merscher, S., Funke, B., Epstein, J. A., Heyer, J., Puech, A., Lu, M. M., Xavier, R. J., Demay, M. B., Russell, R. G., Factor, S. et al. (2001). TBX1 is responsible for cardiovascular defects in velo-cardio-facial/DiGeorge syndrome. *Cell* **104**, 619-629. doi:10.1016/S0092-8674(01)00247-1

Momma, K. (2010). Cardiovascular anomalies associated with chromosome 22q11.2 deletion syndrome. *Am. J. Cardiol.* **105**, 1617-1624. doi:10.1016/j. amjcard.2010.01.333

Morrow, B. E., McDonald-McGinn, D. M., Emanuel, B. S., Vermeesch, J. R. and Scambler, P. J. (2018). Molecular genetics of 22q11.2 deletion syndrome. *Am. J. Med. Genet. A* **176**, 2070-2081. doi:10.1002/ajmg.a.40504

Neubüser, A., Koseki, H. and Balling, R. (1995). Characterization and developmental expression of Pax9, a paired-box-containing gene related to Pax1. *Dev. Biol.* **170**, 701-716. doi:10.1006/dbio.1995.1248

Nishibatake, M., Kirby, M. L. and Van Mierop, L. H. (1987). Pathogenesis of persistent truncus arteriosus and dextroposed aorta in the chick embryo after neural crest ablation. *Circulation* **75**, 255-264. doi:10.1161/01.CIR.75.1.255

Okubo, T., Kawamura, A., Takahashi, J., Yagi, H., Morishima, M., Matsuoka, R. and Takada, S. (2011). Ripply3, a Tbx1 repressor, is required for development of the pharyngeal apparatus and its derivatives in mice. *Development* **138**, 339-348. doi:10.1242/dev.054056

Pabst, O., Rummelies, J., Winter, B. and Arnold, H.-H. (2003). Targeted disruption of the homeobox gene Nkx2.9 reveals a role in development of the spinal accessory nerve. *Development* **130**, 1193-1202. doi:10.1242/dev.00346

Padget, R. L., Mohite, S. S., Hoog, T. G., Justis, B. S., Green, B. E. and Udan, R. S. (2019). Hemodynamic force is required for vascular smooth muscle cell recruitment to blood vessels during mouse embryonic development. *Mech. Dev.* **156**, 8-19. doi:10.1016/j.mod.2019.02.002

Papangeli, I. and Scambler, P. (2013). The 22q11 deletion: DiGeorge and velocardiofacial syndromes and the role of TBX1. *Wiley Interdiscip. Rev. Dev. Biol.* **2**, 393-403. doi:10.1002/wdev.75

Perris, R. and Perissinotto, D. (2000). Role of the extracellular matrix during neural crest cell migration. *Mech. Dev.* **95**, 3-21. doi:10.1016/S0925-4773(00)00365-8

Peters, H., Neubuser, A., Kratochwil, K. and Balling, R. (1998). Pax9-deficient mice lack pharyngeal pouch derivatives and teeth and exhibit craniofacial and limb abnormalities. *Genes Dev.* **12**, 2735-2747. doi:10.1101/gad.12.17.2735

Randall, V., McCue, K., Roberts, C., Kyriakopoulou, V., Beddow, S., Barrett, A. N., Vitelli, F., Prescott, K., Shaw-Smith, C., Devriendt, K. et al. (2009). Great vessel development requires biallelic expression of Chd7 and Tbx1 in pharyngeal ectoderm in mice. *J. Clin. Invest.* **119**, 3301-3310. doi:10.1172/JCI37561

Ritchie, M. E., Phipson, B., Wu, D., Hu, Y., Law, C. W., Shi, W. and Smyth, G. K. (2015). limma powers differential expression analyses for RNA-sequencing and microarray studies. *Nucleic Acids Res.* **43**, e47. doi:10.1093/nar/gkv007

Roberts, L. K. and Gerald, B. (1978). Absence of both common carotid arteries. *Am. J. Roentgenol.* **130**, 981-982. doi:10.2214/ajr.130.5.981

Santen, G. W. E., Sun, Y., Gijsbers, A. C. J., Carré, A., Holvoet, M., Haeringen, A., Lesnik Oberstein, S. A. J., Tomoda, A., Mabe, H., Polak, M. et al. (2012). Further delineation of the phenotype of chromosome 14q13 deletions: (positional) involvement of FOXG1 appears the main determinant of phenotype severity, with no evidence for a holoprosencephaly locus. *J. Med. Genet.* **49**, 366-372. doi:10. 1136/jmedgenet-2011-100721

Scambler, P. J. (2000). The 22q11 deletion syndromes. *Hum. Mol. Genet.* **9**, 2421-2426. doi:10.1093/hmg/9.16.2421

Schmittgen, T. D. and Livak, K. J. (2008). Analyzing real-time PCR data by the comparative C(T) method. *Nat. Protoc.* **3**, 1101-1108. doi:10.1038/nprot.2008.73

Schneider, J. E., Böse, J., Bamforth, S. D., Gruber, A. D., Broadbent, C., Clarke, K., Neubauer, S., Lengeling, A. and Bhattacharya, S. (2004). Identification of cardiac malformations in mice lacking Ptdsr using a novel high-throughput magnetic resonance imaging technique. *BMC Dev. Biol.* **4**, 16. doi:10.1186/1471-213X-4-16

Soriano, P. (1999). Generalized lacZ expression with the ROSA26 Cre reporter strain. *Nat. Genet.* **21**, 70-71. doi:10.1038/5007

Srinivas, S., Watanabe, T., Lin, C.-S., William, C. M., Tanabe, Y., Jessell, T. M. and Costantini, F. (2001). Cre reporter strains produced by targeted insertion of EYFP and ECFP into the ROSA26 locus. *BMC Dev. Biol.* **1**, 4. doi:10.1186/1471-213X-1-4

Subramanian, A., Tamayo, P., Mootha, V. K., Mukherjee, S., Ebert, B. L., Gillette, M. A., Paulovich, A., Pomeroy, S. L., Golub, T. R., Lander, E. S. et al. (2005). Gene set enrichment analysis: a knowledge-based approach for interpreting genome-wide expression profiles. *Proc. Natl Acad. Sci. USA* **102**, 15545-15550. doi:10.1073/pnas.0506580102

DEVELOPMENT

Sun, Q., Liu, S., Liu, K. and Jiao, K. (2018). Role of Semaphorin signaling during cardiovascular development. *J. Am. Heart Assoc.* **7**, e008853. doi:10.1161/JAHA. 118.008853

Thom, T., Haase, N., Rosamond, W., Howard, V. J., Rumsfeld, J., Manolio, T., Zheng, Z. J., Flegal, K., O'Donnell, C., Kittner, S. et al. (2006). Heart disease and stroke statistics–2006 update: a report from the American Heart Association Statistics Committee and Stroke Statistics Subcommittee. *Circulation* **113**, e85-e151. doi:10.1161/circulationaha.105.171600

Unolt, M., Versacci, P., Anaclerio, S., Lambiase, C., Calcagni, G., Trezzi, M., Carotti, A., Crowley, T. B., Zackai, E. H., Goldmuntz, E. et al. (2018). Congenital heart diseases and cardiovascular abnormalities in 22q11.2 deletion syndrome: From well-established knowledge to new frontiers. *Am. J. Med. Genet. A* **176**, 2087-2098. doi:10.1002/ajmg.a.38662

van Bueren, K. L., Papangeli, I., Rochais, F., Pearce, K., Roberts, C., Calmont, A., Szumska, D., Kelly, R. G., Bhattacharya, S. and Scambler, P. J. (2010). Hes1 expression is reduced in Tbx1 null cells and is required for the development of structures affected in 22q11 deletion syndrome. *Dev. Biol.* **340**, 369-380. doi:10.1016/j.ydbio.2010.01.020

Van Mierop, L. H. S. and Kutsche, L. M. (1986). Cardiovascular anomalies in digeorge syndrome and importance of neural crest as a possible pathogenetic factor. *Am. J. Cardiol.* **58**, 133-137. doi:10.1016/0002-9149(86)90256-0

Waldo, K. L., Kumiski, D. and Kirby, M. L. (1996). Cardiac neural crest is essential for the persistence rather than the formation of an arch artery. *Dev. Dyn.* **205**, 281-292. doi:10.1002/(SICI)1097-0177(199603)205:3<281::AID-AJA8>3.0. CO;2-E

Xu, H., Morishima, M., Wylie, J. N., Schwartz, R. J., Bruneau, B. G., Lindsay, E. A. and Baldini, A. (2004). Tbx1 has a dual role in the morphogenesis of the cardiac outflow tract. *Development* **131**, 3217-3227. doi:10.1242/dev.01174

Yagi, H., Furutani, Y., Hamada, H., Sasaki, T., Asakawa, S., Minoshima, S., Ichida, F., Joo, K., Kimura, M., Imamura, S.-I. et al. (2003). Role of TBX1 in human del22q11.2 syndrome. *Lancet* **362**, 1366-1373. doi:10.1016/S0140-6736(03)14632-6

Yashiro, K., Shiratori, H. and Hamada, H. (2007). Haemodynamics determined by a genetic programme govern asymmetric development of the aortic arch. *Nature* **450**, 285-288. doi:10.1038/nature06254

Zhang, Z. and Baldini, A. (2008). In vivo response to high-resolution variation of Tbx1 mRNA dosage. *Hum. Mol. Genet.* **17**, 150-157. doi:10.1093/hmg/ddm291

Zhang, Z., Cerrato, F., Xu, H., Vitelli, F., Morishima, M., Vincentz, J., Furuta, Y., Ma, L., Martin, J. F., Baldini, A. et al. (2005). Tbx1 expression in pharyngeal epithelia is necessary for pharyngeal arch artery development. *Development* **132**, 5307-5315. doi:10.1242/dev.02086

Zweier, C., Sticht, H., Aydin-Yaylagül, I., Campbell, C. E. and Rauch, A. (2007). Human TBX1 missense mutations cause gain of function resulting in the same phenotype as 22q11.2 deletions. *Am. J. Hum. Genet.* **80**, 510-517. doi:10.1086/511993

DEVELOPMENT

Supplementary Figures

Figure S1. Pax9 expression during mouse pharyngeal development. A – C, coronal, and **D – F,** transverse sections of embryos at E9.5 (**A**), E10.5 (**B**), E11.5 (**C, D**), E12.5 (**E**) and E15.5 (**F**). Pharyngeal arch arteries (paa) are outlined. Pax9 is expressed in the pharyngeal endoderm at E9.5 and E10.5, and is subsequently expressed within the esophagus (es), developing thymus (th) and ultimobranchial bodies (ub) of the pharyngeal region. Somite counts (s) indicated. Abbreviations: L/R-4th, left/right 4th pharyngeal arch artery; lcc, left common carotid; oft, outflow tract; pa, pharyngeal arch; pp, pharyngeal pouch; ph, pharynx; rcc, right common carotid; tr, trachea. Scale, 100μm.
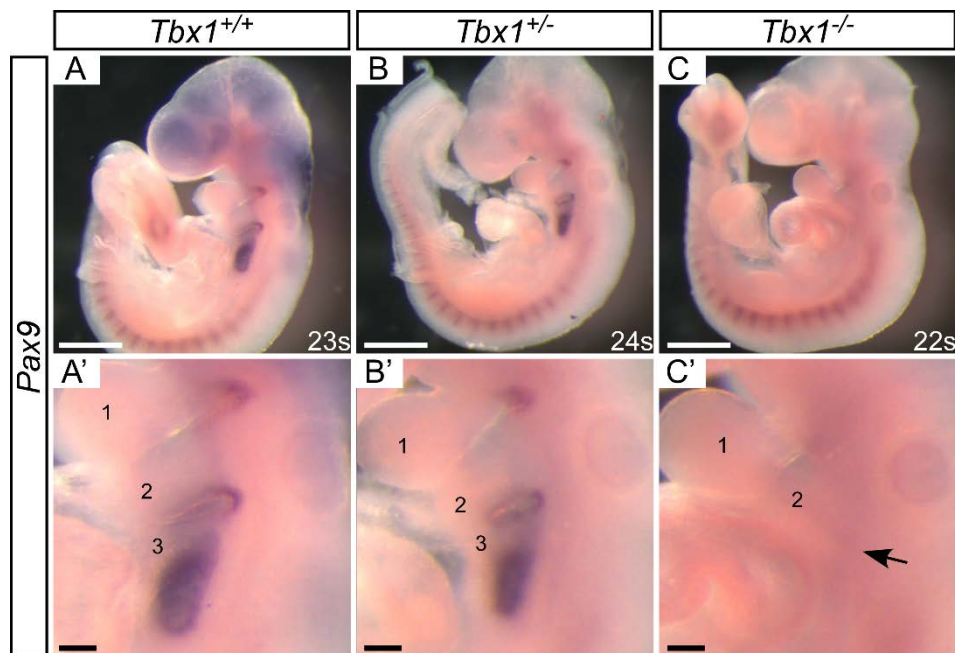
Figure S2. *Pax9* mRNA is reduced in the pharyngeal region of *Tbx1⁻/⁻* embryos. Whole-mount *in situ* hybridization using a *Pax9* riboprobe demonstrates that *Pax9* is specifically expressed in the pharyngeal endoderm and somites at E9.5 in wild-type (**A**) and *Tbx1⁺/⁻* (**B**) embryos. **C,** In *Tbx1⁻/⁻* embryos, however, *Pax9* levels are dramatically reduced from the pharyngeal endoderm (*arrow*). Somite counts (s) indicated. Scale: A – C, 500µm; A' – C', 100µm.

Direction of change in
***Tbx1-Pax9* shared genes**
(n=329)

Gene up or down per dataset	Concordant		Discordant	
	Tbx1 up, *Pax9* up	*Tbx1* down, *Pax9* down	*Tbx1* up, *Pax9* down	*Tbx1* down, *Pax9* up
n	2	114	7	207
Examples of genes in each category	*Cisd2, CxCl13*	*Aldh1a1, Gbx2, Gli3, Myh9, Notch3, Pax9, Pbx1, Tbx1*	*Col3a1, Col6a1, Kif1b, Sparcl1, Vtn*	*Bmp5, Bnip3, Cdkn1b, Cldn12, Dlx6, Fgfr1op2, Hes1*

■ *Tbx1* up, *Pax9* up

■ *Tbx1* down, *Pax9* down

■ *Tbx1* up, *Pax9* down

■ *Tbx1* down, *Pax9* up

Figure S3. Relationship between shared genes differentially expressed in *Tbx1*-null and *Pax9*-null datasets. Shared genes (n=329) between the *Tbx1*-null and *Pax9*-null datasets were compared to see if they were concordant (i.e. genes went up in both datasets, or down), or if they were discordant (i.e. went up in one dataset but down in the other). This revealed that 35% of shared genes were both down, but also 63% of shared genes were down in *Tbx1*-nulls and up in *Pax9*-nulls. Examples of genes in each category are shown in the **Table**.
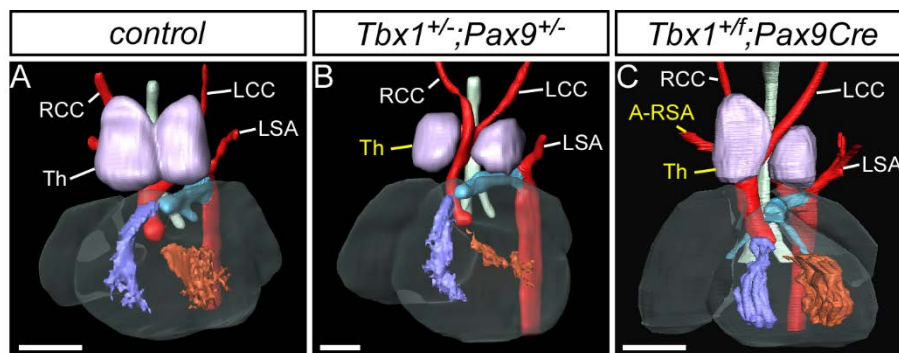
Figure S4. Thymus abnormalities are seen in *Tbx1;Pax9* mutant embryos.
An abnormally placed thymus was frequently observed in conjunction with arch artery defects. **A,** Normally placed thymic lobes (*purple*) in a wild-type control embryo. The thymic lobes are placed ventrally to the aortic arch arteries. **B, C,** In a *Tbx1+/−;Pax9+/−* mutant embryo (**B**) and a *Tbx1+/−;Pax9Cre* mutant embryo (**C**), both with interrupted aortic arch and aberrant right subclavian artery (A-RSA), the thymic lobes are split and asymmetrically placed. The right and left common carotid arteries can be seen traversing between the two thymic lobes. Abbreviations: LCC, left common carotid; LSA, left subclavian artery; RCC, right common carotid; Th, thymus. Scale, 500µm.
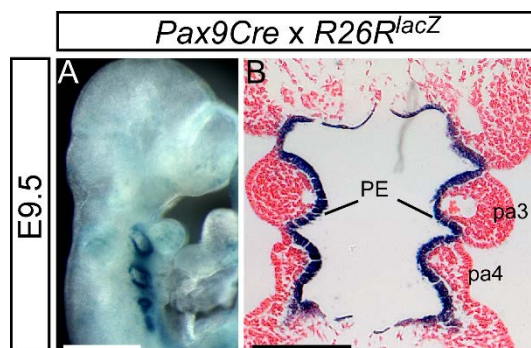
Figure S5. Reporter gene expression from the *Pax9Cre* allele.
A, B, Cre mediated recombination of *lacZ* by *Pax9Cre* induces expression in the pharyngeal endoderm at E9.5. Scale, 500 µm.

Supplementary Tables

Table S1 (Excel file). Differentially expressed genes ($p \le 0.1$) from RNA-seq analysis of *Pax9*-null pharyngeal arch tissue. **Sheet A, B,** The top up- and down-regulated coding genes from the *Pax9* RNA-seq data are listed and ranked by log2 fold-change, with a cut off -0.59 for the down-regulated genes (**A**; n=647) and 0.59 for the up-regulated genes (**B**; n=240).
Sheet C, D, Values of the *Tbx1-Pax9* shared genes from the *Pax9* RNA-seq data, ranked by fold-change. **C**, Genes down-regulated in *Pax9*-null pharyngeal arch tissue (n=122). **D,** Genes up-regulated in *Pax9*-null pharyngeal arch tissue (n=220).

Click here to Download Table S1

Table S2. Genotypes of weaned pups (at 3 weeks of age), neonates (collected within 24 h of birth) and embryos (E15.5 and E9.5) from a $Tbx1^{+/-}$ and $Pax9^{+/-}$ cross. There was a significant loss of expected pups at weaning (Chi-squared test; **** $p=1.4\times10^{-12}$). There was no significant difference from the expected number of pups for each possible genotype in neonates or embryos.

Genotype	Weaning	Neonate	E15.5	E9.5
Wild-type	55	7	16	20
Pax9⁺/⁻	68	10	15	14
Tbx1⁺/⁻	43	6	19	17
Tbx1⁺/⁻;Pax9⁺/⁻	2 ****	9	20	23
Total	*168*	*32*	*70*	*74*
n expected for each genotype	42	8.0	17.5	18.5

Table S3. Summary of thymus phenotypes observed in *Tbx1* and *Tbx1;Pax9* mutant embryos. The thymus was frequently seen to be asymmetric in appearance and split apart in *Tbx1⁺/⁻;Pax9⁺/⁻* and *Tbx1⁺/ᶠˡᵒˣ;Pax9Cre* mutants. An abnormal thymus was always associated with an arch artery defect. One *Tbx1⁺/⁻;Pax9⁺/⁻* mutant presented with an absent thymus and an unusual holoprosencephaly type phenotype (not shown).

Genotype	Stage	*n*	Thymus phenotype		
			Normal	Split & asymmetric	Absent
Tbx1⁺/⁻	E15.5	19	15 (79%)	4 (21%)	0
Tbx1⁺/⁻;Pax9⁺/⁻		20	3 (15%)	16 (80%)	1 (5%)
Tbx1⁺/ᶠˡᵒˣ;Pax9Cre	E13.5 -E15.5	26	16 (61.5%)	10 (38.5%)	0

Table S4. Genotypes of neonates (collected within 48 h of birth) from a *Tbx1$^{+/flox}$* x *Pax9Cre* cross. Foetuses (E13.5 – E15.5) and embryos (E10.5) were from a *Tbx1$^{flox/flox}$* x *Pax9Cre* cross. There was a significant loss of expected neonates (Chi-squared test; **** *p*=2.4x10^{-5}).

Genotype	Neonate	Foetus	Embryo
Wild-type	39	-	-
Pax9Cre	43	-	-
Tbx1$^{+/flox}$	33	18	15
Tbx1$^{+/flox}$;Pax9Cre	8****	17	17
Total	*123*	*35*	*32*
n expected for each genotype	30.75	17.5	16

Table S5. *PAX9* mutations and aberrant expression levels that have been associated with human disease.

Disease	Mutation/ karyotype	Detail	Other	Reference
Congenital Heart Defect	14q13 (105kb deletion)	IAA-B, BAV, hypoplastic aorta, VSD	Facial dysmorphisms	[1]
	46,XY,del(14) (11.2q13)	Persistent foramen ovale	Craniofacial defects	[2]
	46,XY,del(14) (11.2q13)	Patent foramen ovale and patent ductus arteriosus	Craniofacial defects, delayed bone ossification	[3]
	14q13.3 (884kb deletion)	Persistent pulmonary hypertension of the newborn	Oligodontia, hypothyroidism	[4]
Craniofacial	*PAX9* mutations	Hypo/oligodontia	-	[5,6]
		Cleft lip/palate	Hypodontia	[7,8]
Skeletal	46,XY,t(14;18) (q13;q12)	Mesomelic bone dysplasia	-	[9]
	Jarcho-Levin Syndrome	Vertebral segmentation defect	Reduction in PAX9 expression	[10]
Cancer	14q13.3	Lung cancer	PAX9 expression amplified	[11]

PAX9 is located at 14q13.3.
Abbreviations: BAV, bicuspid aortic valve; IAA-B, interrupted aortic arch type B; VSD, ventricular septal defect.

Table S6. Penetrance of 4th PAA defects in *Tbx1+/–* and *Tbx1+/flox;Pax9Cre* mutant embryos assessed from published and our data.

Genotype	Stage	n	% defects [a]	Reference
Tbx1+/–	E10.5–E11.0	127	87% (63-100%)	[12-17] & this study
	E11.5	76	62% (50-74%)	[16-18]
	Fetal (E14.5–P2)	215	34% (18-49%)	[12-16,18-20] & this study
Tbx1+/flox; Pax9Cre	E10.5	17	92%	This study
	Fetal (E13.5–E15.5)	18	33%	This study

[a] For *Tbx1+/–* mice, % defects are given as the mean incidence of abnormalities for the studies cited, with 95% confidence intervals.

Table S7. Penetrance of 4th PAA defects following heterozygous deletion of *Tbx1* (globally or conditionally) from E10.5 embryos and assessed by intra-cardiac ink injection from published and our data.

Genotype	Tissue affected	n	Abnormal	Reference
Tbx1+/–	Endoderm, mesoderm, ectoderm	127	87%	[12-17] & this study
Tbx1+/–; Pax9+/–	Endoderm, mesoderm, ectoderm	9	100%	This study
Tbx1+/flox; Pax9Cre	Endoderm	17	92%	This study
Tbx1+/flox; Foxg1Cre	Endoderm*	30	0	[21]
Tbx1+/flox; Mesp1Cre	Mesoderm	19	0	[22]
Tbx1+/flox; Foxg1Cre	Endoderm, mesoderm, ectoderm	21	42%	[22]
Tbx1+/flox; Fgf15Cre	Endoderm, ectoderm	34	20%	[22]
Tbx1+/flox; Hoxa3Cre	Endoderm, mesoderm, ectoderm (neural crest)	17	50%	[22]
*Tbx1+/flox; AP2aCre**	Ectoderm (neural crest)	9	0	[14]

* Mice were maintained congenic in the Swiss Webster background to restrict Cre expression to the pharyngeal endoderm.
** *Tbx1+/flox;AP2aCre* phenotype assessed at E15.5 by histology.
N.B. *Tbx1* is not expressed in neural crest cells.

Table S8. Antibodies and probes used for immunostaining and *in situ* hybridisation.

Target	Catalogue number	Species and type	Supplier	Dilution
Primary antibodies				
Pax9	ab28538	Rat monoclonal	Abcam	1:100
Tbx1	ab18530	Rabbit polyclonal		1:100
CD31	ab56299	Rat monoclonal		1:100
GFP	ab6556	Rabbit polyclonal		1:100
ERG	ab92513	Rabbit monoclonal		1:1000
BrDU	ab6326	Rat monoclonal		1:200
Cleaved caspase-3	9661	Rabbit polyclonal	Cell Signalling	1:300
aSMA	a2547	Mouse monoclonal	Sigma	1:200
Secondary antibodies				
Donkey anti-mouse IgG Alexa Fluor 488	A-21202	-	Thermo Fisher Scientific	1:200
Donkey anti-rabbit IgG Alexa Fluor 488	A-21206	-		
Donkey anti-rabbit IgG Alexa Fluor 594	A-21207	-		
Donkey anti-rat IgG Alexa Fluor 488	A-21208	-		
Donkey anti-rat IgG Alexa Fluor 594	A-21209	-		
Goat anti-rat IgG Alexa Fluor 647	A-21247	-		
Nuclear stain				
DAPI	H-1200	-	Vector Laboratories	-
RNAscope probes				
Pax9	454321-C2	Mouse	Advanced Cell Diagnostics	1:50
Tbx1	481911			Direct
Chd7	458031			Direct
Gbx2	314358			1:50

Table S9. qPCR primer sequences

Gene	RefSeq	Primer sequence
Chd7	NM_001081417	GGAGAACCCTGAGTTTGCTG CCCTGAAGTAGAGGCGACAG
eYFP	-	ACGTAAACGGCCACAAGTTC TCGTCCTTGAAGAAGATGGTG
Gapdh	NM_008084	TGTGCAGTGCCAGCCTCGTC TGACCAGGCGCCCAATACGG
Gbx2	NM_010262	GAGGCGGCAACTTCGACAAAGCC TCCTCCTTGCCCTTCGGGTCATC
Pax9	NM_011041	CCGGCACAGACTTCCTTTTA CCTTCCGTTCACGAACACTC
Tbx1	NM_011532	TGAGGAGACACGCTTCACTG CTGCAGCGTCTTTGTCTGAG

References

1. Santen, G.W. *et al.* Further delineation of the phenotype of chromosome 14q13 deletions: (positional) involvement of FOXG1 appears the main determinant of phenotype severity, with no evidence for a holoprosencephaly locus. *J Med Genet* **49**, 366-72 (2012).

2. Schuffenhauer, S. *et al.* De novo deletion (14)(q11.2q13) including PAX9: clinical and molecular findings. *J Med Genet* **36**, 233-236 (1999).

3. Shapira, S.K. *et al.* De novo proximal interstitial deletions of 14q: cytogenetic and molecular investigations. *Am J Med Genet* **52**, 44-50 (1994).

4. Hayashi, S., Yagi, M., Morisaki, I. & Inazawa, J. Identical deletion at 14q13.3 including PAX9 and NKX2-1 in siblings from mosaicism of unaffected parent. *J Hum Genet* (2015).

5. Stockton, D.W., Das, P., Goldenberg, M., D'Souza, R.N. & Patel, P.I. Mutation of PAX9 is associated with oligodontia. *Nature Genetics* **24**, 18-19 (2000).

6. Bonczek, O., Balcar, V.J. & Šerý, O. PAX9 gene mutations and tooth agenesis: A review. *Clinical Genetics* **92**, 467-476 (2017).

7. Das, P. *et al.* Novel missense mutations and a 288-bp exonic insertion in PAX9 in families with autosomal dominant hypodontia. *American Journal of Medical Genetics Part A* **118A**, 35-42 (2003).

8. Ichikawa, E. *et al.* PAX9 and TGFB3 are linked to susceptibility to nonsyndromic cleft lip with or without cleft palate in the Japanese: population-based and family-based candidate gene analyses. *Journal Of Human Genetics* **51**, 38 (2005).

9. Kamnasaran, D. *et al.* Defining the breakpoints of proximal chromosome 14q rearrangements in nine patients using flow-sorted chromosomes. *Am J Med Genet* **102**, 173-82 (2001).

10. Bannykh, S.I. *et al.* Aberrant Pax1 and Pax9 expression in Jarcho-Levin syndrome: Report of two Caucasian siblings and literature review. *American Journal of Medical Genetics Part A* **120A**, 241-246 (2003).

11. Kendall, J. *et al.* Oncogenic cooperation and coamplification of developmental transcription factor genes in lung cancer. *Proceedings of the National Academy of Sciences* **104**, 16663-16668 (2007).

12. Calmont, A. *et al.* Tbx1 controls cardiac neural crest cell migration during arch artery development by regulating Gbx2 expression in the pharyngeal ectoderm. *Development* **136**, 3173-3183 (2009).

13. Guris, D.L., Duester, G., Papaioannou, V.E. & Imamoto, A. Dose-dependent interaction of Tbx1 and Crkl and locally aberrant RA signaling in a model of del22q11 syndrome. *Dev Cell* **10**, 81-92 (2006).

14. Randall, V. *et al.* Great vessel development requires biallelic expression of Chd7 and Tbx1 in pharyngeal ectoderm in mice. *J Clin Invest* **119**, 3301-10 (2009).

15. Vitelli, F., Morishima, M., Taddei, I., Lindsay, E.A. & Baldini, A. Tbx1 mutation causes multiple cardiovascular defects and disrupts neural crest and cranial nerve migratory pathways. *Hum Mol Genet* **11**, 915-22 (2002).

16. Ryckebusch, L. *et al.* Decreased Levels of Embryonic Retinoic Acid Synthesis Accelerate Recovery From Arterial Growth Delay in a Mouse Model of DiGeorge Syndrome. *Circ Res* **106**, 686-694 (2010).

17. Lindsay, E.A. & Baldini, A. Recovery from arterial growth delay reduces penetrance of cardiovascular defects in mice deleted for the DiGeorge syndrome region. *Hum Mol Genet* **10**, 997-1002 (2001).

18. Papangeli, I. & Scambler, P.J. Tbx1 genetically interacts with the transforming growth factor-beta/bone morphogenetic protein inhibitor Smad7 during great vessel remodeling. *Circ Res* **112**, 90-102 (2013).

19. Zhang, Z. & Baldini, A. In vivo response to high-resolution variation of Tbx1 mRNA dosage. *Hum Mol Genet* **17**, 150-7 (2008).

20. Aggarwal, V.S. *et al.* Dissection of Tbx1 and Fgf interactions in mouse models of 22q11DS suggests functional redundancy. *Hum Mol Genet* **15**, 3219-28 (2006).

21. Arnold, J.S. *et al.* Inactivation of Tbx1 in the pharyngeal endoderm results in 22q11DS malformations. *Development* **133**, 977-87 (2006).

22. Zhang, Z. *et al.* Tbx1 expression in pharyngeal epithelia is necessary for pharyngeal arch artery development. *Development* **132**, 5307-15 (2005).